(2)

AD-A250 711

# TATION PAGE

Form Approved
OMB No. 0704-0188



| 2. REPORT DATE | 3. REPORT TYPE AND DATES COVERED |
|---|---|
| 5/92 | Annual Feb. 1991 - Jan. 1992 |

**4. TITLE AND SUBTITLE**
Interactive Control in Turbulent Shear Layers
(U)

**5. FUNDING NUMBERS**
PE - 61102F
PR - 2307
SA - BS
G - AFOSR-90-0171

**6. AUTHOR(S)**
Candace E. Wark
Hassan M. Nagib

**7. PERFORMING ORGANIZATION NAME(S) AND ADDRESS(ES)**
Illinois Institute of Technology
Fluid Dynamics Research Center
3110 S. State Street
Chicago, IL 60616

NA

**8. PERFORMING ORGANIZATION REPORT NUMBER**
AFOSR-TR 92 0514

**9. SPONSORING/MONITORING AGENCY NAME(S) AND ADDRESS(ES)**
AFOSR/NA
Building 410
Bolling AFB DC 20332-6448



**10. SPONSORING/MONITORING AGENCY REPORT NUMBER**
AFOSR-90-0171

**11. SUPPLEMENTARY NOTES**

**12a. DISTRIBUTION/AVAILABILITY STATEMENT**
Approved for public release; distribution is unlimited

**12b. DISTRIBUTION CODE**
*Original contains color plates: All DTIC reproductions will be in black and white*

**13. ABSTRACT (Maximum 200 words)**

Using Particle Image Velocimetry in a turbulent pipe flow, instantaneous large-scale structures were observed, which are not seen in low Reynolds number direct numerical simulations of bounded turbulent shear flow. A probable explanation for this discrepancy is the much larger experimental Reynolds number as compared with the DNS results. Further support of this Reynolds number influence was found when quantifying the relative role of the outer-layer structures and wall-layer structures on the spanwise correlation coefficient between the wall-shear stress and streamwise velocity. That is, the results suggest that the influence of the outer flow on the streamwise velocity fluctuations at $y^+ = 10$, increases with increasing Reynolds number. This outer-layer effect was then further examined in terms of the boundary layer intermittency/wall-layer dynamics coupling. Although the outer layer is directly influencing the wall-layer region, it was found that the alternating passages of laminar and turbulent regions in the intermittent part of the boundary layer were not directly influencing the buffer layer statistics. The mechanisms of this influence are currently being investigated.

**14. SUBJECT TERMS**
Coherent Structures
Turbulent Boundary Layers
Reynolds Number Scaling

**15. NUMBER OF PAGES**
30

**16. PRICE CODE**

| 17. SECURITY CLASSIFICATION OF REPORT | 18. SECURITY CLASSIFICATION OF THIS PAGE | 19. SECURITY CLASSIFICATION OF ABSTRACT | 20. LIMITATION OF ABSTRACT |
|---|---|---|---|
| Unclassified | Unclassified | Unclassified | UL |

# INTERACTIVE CONTROL IN TURBULENT SHEAR LAYERS

## SECOND ANNUAL TECHNICAL REPORT

## AFOSR-90-0171


**INVESTIGATORS:**

Candace E. Wark
Hassan M. Nagib




February 1991 - January 1992


**ILLINOIS INSTITUTE OF TECHNOLOGY**

Fluid Dynamics Research Center
&
Mechanical and Aerospace Engineering Department

Chicago, Illinois 60616

# TABLE OF CONTENTS

## Interactive Control in Turbulent Shear Layers

### I. Introduction

Distinctive features of a wall-bounded turbulent shear flow include its three-dimensional rotational nature, the production of turbulent kinetic energy and momentum exchange between the wall-layer and the outer-layer. General characteristics of both the wall-layer and outer-layer have been extensively studied using various detection techniques and intermittency schemes. The conditional or ensemble-averaged spatial structures associated with several of these techniques have been documented. However, there is considerable controversy regarding the extension of these ensemble-averaged results to the instantaneous flow field. To date, the only documentation available of the instantaneous velocity field in a bounded turbulent shear flow is from the direct numerical simulation results of Stanford/NASA Ames. However, these are limited to very low Reynolds numbers which are not characteristic of practical engineering problems.

One of the fundamental approaches in the study of turbulent boundary layers is to investigate the scaling of turbulent quantities. Successful scaling of a turbulent quantity with either wall or outer scales implies that the dynamics of the turbulent motion(s) producing the given quantity is controlled by the wall layer or outer region of the boundary layer respectively. McLean (1990) and Wark et al. (1991) both concluded that, even as close to the wall as $y^+ = 10$, the outer layer had an influence on the spanwise two-point correlation function. Nevertheless, the features or mechanisms of the outer flow influencing the wall layer are not understood. Also, the quantification of the outer-layer influence and Reynolds number dependence would be a significant contribution to understanding turbulent boundary layer dynamics.

The instantaneous state of the flow field for higher Reynolds numbers than those available by Direct Numerical Simulation has been investigated in various flow visualization experiments. Flow visualization by Smith and Metzler (1983) showed that low-speed streaks seem to be independent of Reynolds number for $740 < Re_\theta < 5830$. Also many investigators have isolated components of the hairpin vortex, such as the streamwise vortices or the spanwise vortices forming the head and have conjectured as to their relation with the hairpin vortex, but have failed to provide substantial evidence linking all of the hairpin vortex component together in a fully turbulent boundary layer.

The results of the past year have attempted to understand the relation between the intermittent outer layer flow with the wall-layer dynamics as well as to quantify the relative roles of the inner and outer layer and determine if a Reynolds number effect exists. Also two and three dimensional views of the turbulence in the wall region were recorded on high speed film simultaneously with the wall-shear signal at an $Re_\theta$ of 2100.

## II. Structure of Turbulence Using PIV in a Wall-Bounded Shear Flow

Many recent investigations of wall-bounded turbulent shear flow have focused on the statistics and structure of turbulence with emphasis on the Reynolds number dependence. Most of the experimental investigations have relied upon single-point measurements; whereas, Direct Numerical Simulation (DNS) results provide full-field information in a three-dimensional grid for various turbulent shear flows. However, these results are limited to very low Reynolds numbers. A promising technique for obtaining high Reynolds number, full-field information is Particle Image Velocimetry (PIV) (see Adrian 1991).

Experimental Procedure. A fully-developed turbulent pipe flow in air at $Re_D$ = 50,000 was investigated using PIV. The pipe was 127mm in diameter and the measurement location was 155 pipe diameters downstream from the pipe inlet. The data acquisition system consisted of a pair of Nd-YAG lasers with approximately 75mJ of energy per pulse at a wavelength of 532nm. Each laser was pulsed at 50Hz, and a SRS 435 digital delay generator was used to achieve a 46$\mu$sec time delay between the two laser pulse trains. The photographs were double exposed and recorded using a 4" by 5" view camera. A Nikon 135mm Nikor lens at f/8 was used to record particle images with a magnification of 1:1 on TMAX 400 film. The flow was seeded with atomized olive-oil droplets approximately 1 to 5$\mu$m in diameter.

Results. Eleven photographs were analyzed, using the direct autocorrelation technique (see Adrian 1991), in a 1mm by 1mm interrogation spot, with a 0.5mm grid spacing between interrogation spots. The number of particle pairs in each interrogation spot was typically between 10 and 20. This yielded velocity vectors at approximately 9,000 x-y locations. Each of the eleven instantaneous realizations span 1800 wall units in the streamwise direction and extend from $y^+ = 10$ to $y^+ \approx 300$: the centerline of the pipe corresponds to $y^+ = 1{,}300$.

The line-averaged mean velocity profile resulting from the eleven photographs is given in the top plot of Figure 1. The solid line represents the log-law velocity profile and excellent collapse is seen for all data except for $y^+ = 10$. A plausible explanation for the over-estimation of the mean streamwise velocity at $y^+ = 10$ is that fewer particles were observed as one approached the wall. Therefore, close to the wall, the velocity would be biased towards the particles located at higher $y^+$ positions within each interrogation spot; thus, resulting in a bias towards higher velocities. The bottom plot in Figure 1 is taken from Lekakis (1988) at the same Reynolds number in the same facility. The solid line is the same log-law fit and the agreement between the PIV data and hot-wire data (except for $y^+ = 10$) is evident by comparing the top and bottom plots. Also the comparison between the rms value for the streamwise velocity component was observed to be in excellent agreement with the hot-wire data from Lekakis (1988).

Figure 2 represents the fluctuating streamwise and normal velocity vectors for one of the eleven photographs. Figure 2a represents a relatively random flow

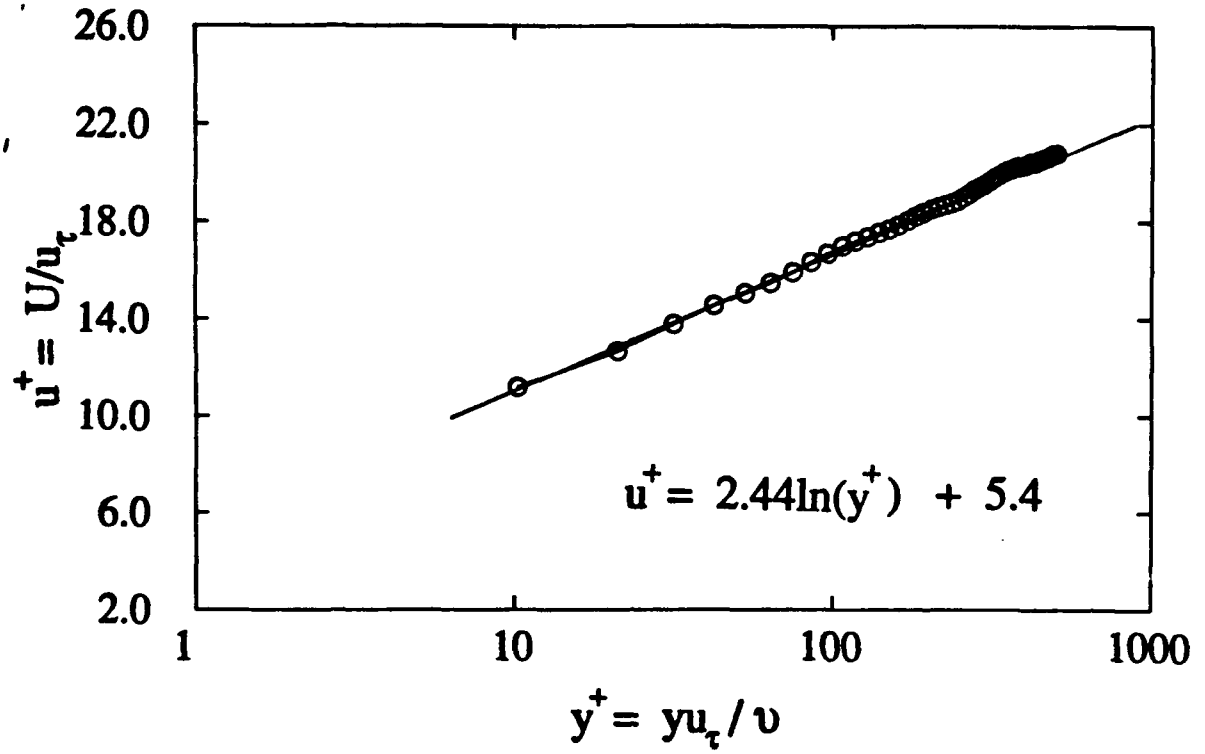


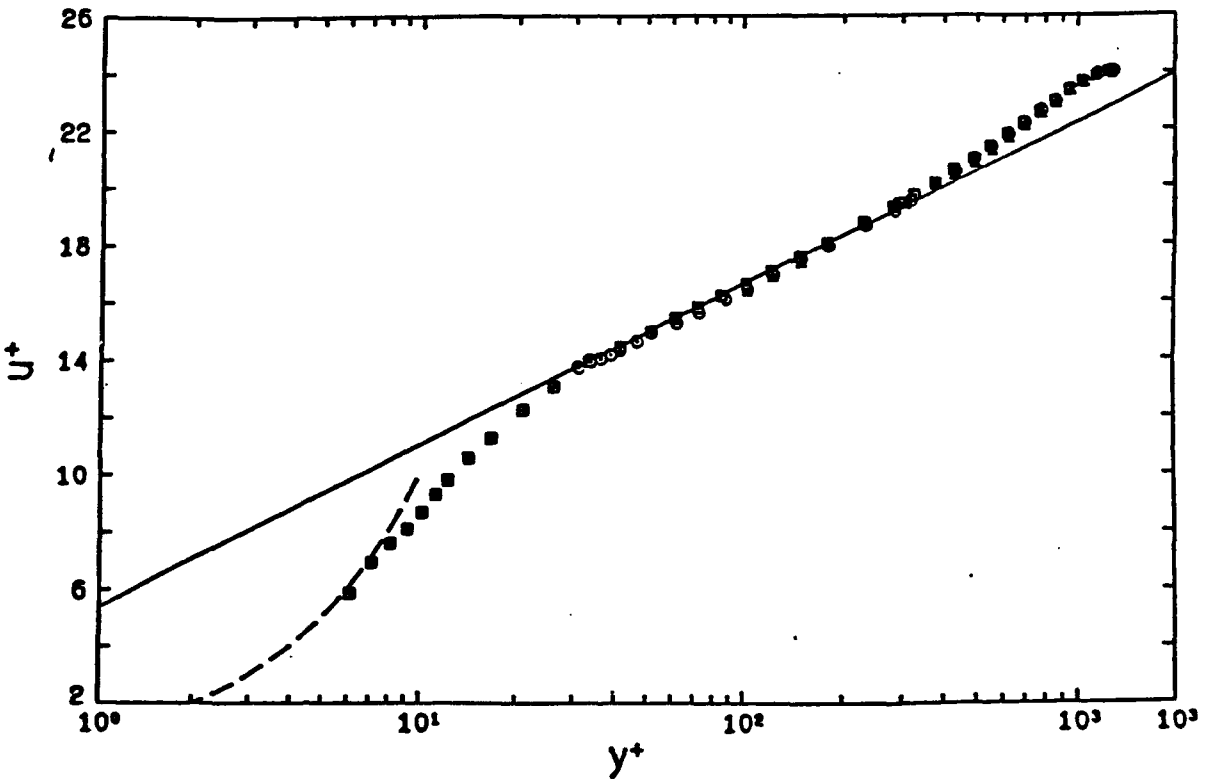


Figure 1. Comparison of the mean u-velocity profile obtained from PIV data (circles) (top plot) with measurements (bottom: taken from Lekakis, 1988) using single, X- and triple hot-film probes. $Re_D$ = 50000, squares - single wire, circles - X wire, triangles - triple wire; _____ $u^+ = 2.44 \ln(y^+) + 5.4$; - - - - - - - $u^+ = y^+$.

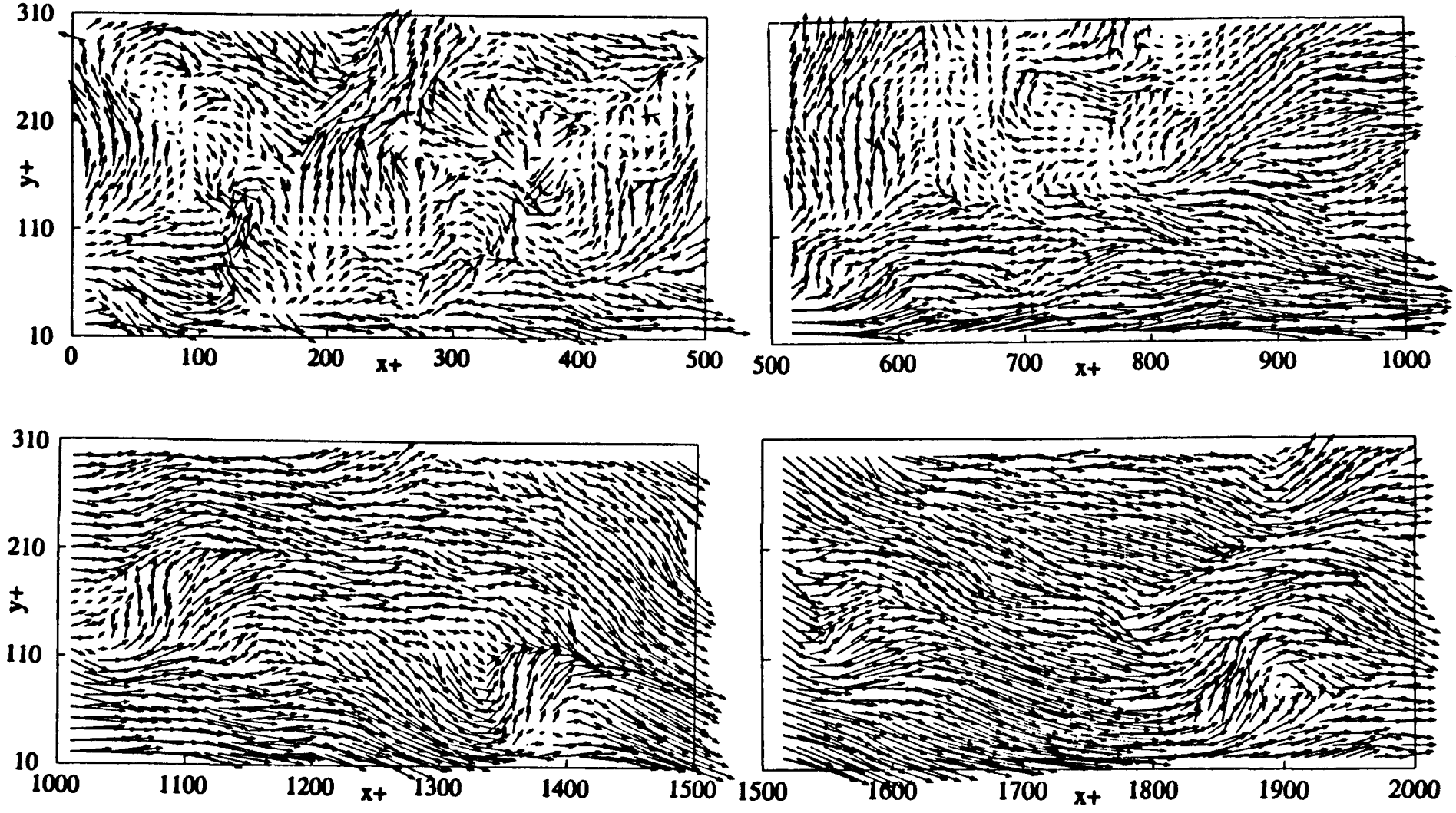


Figure 2. Instantaneous Fluctuating Velocity Vectors in the x-y plane obtained from one photograph. a) $0 \leq x^+ \leq 500$ b) $500 \leq x^+ \leq 1000$ c) $1000 \leq x^+ \leq 1500$ d) $1500 \leq x^+ \leq 2000$.

field with vortices which appear to have length scales on the order of 100 wall units. Proceeding downstream (Figures 2b - 2d) it is evident that a much larger motion with a scale on the order of the pipe diameter, is dominating the velocity vector field.

This is in contrast to the instantaneous realizations obtained from the DNS results from NASA Ames/Stanford (see Robinson 1991). The DNS results resemble more closely the data in Figure 2a but do not depict the large-scale structures which are experimentally observed in Figures 2b-2d. There is a significant difference between the DNS and the present experiment; that is, the $y^+$ at the outer edge of the DNS boundary layer is approximately equal to 350 whereas $y^+$ at the centerline of the pipe is 1300. Also, the numerical box used in the DNS calculations is 4900 wall units in the streamwise direction and since periodic boundary conditions are used these large-scale structures might not be allowed to develop in the simulations.

Further evidence that this apparent discrepancy could be a Reynolds number effect is given by the results of Naguib and Wark (1992). They used a conditional averaging scheme to investigate the ensemble-averaged spatial structure associated with a quadrant detection at $y^+ = 35$ in a turbulent boundary layer. Two Reynolds numbers were investigated, $Re_\theta = 1650$ and 4620: the $y^+$ at the edge of the boundary layer for these two Reynolds numbers was 640 and 1600 respectively. Figures 3 represents the Reynolds-number effect upon the ensemble-averaged structure, when normalized by wall units, for both a Q4 (sweep) detection. A dramatic Reynolds-number effect is seen on the ensemble-averaged structure for both detections.

The $Re_\theta = 4620$ conditions of Naguib and Wark are comparable to the present pipe flow conditions in the sense that $y^+$ at the edge of their turbulent boundary layer is approximately equal to the $y^+$ at the centerline of the pipe. The ensemble-averaged structures of Naguib and Wark are both qualitatively and quantitatively similar in scale to the present instantaneous structures.

Figure 4 represents the results from another of the eleven photographs. The top plot is a comparison of the line-averaged velocity profile for the photograph (in red) with the line-averaged velocity profile for all eleven photographs (black curve). The mean profile for the photo is less in magnitude as compared with the "true" mean and this is easily seen when looking at the instantaneous fluctuating velocity vectors in the bottom plot. The entire photograph is represented; thus, the velocity vectors have been color-coded based on the quadrant scheme to more easily see regions of high and low-speed fluid. A high-speed region extending from the wall to $y^+ > 300$ is observed directly upstream of a large-scale low-speed region.

Conclusions. Statistics computed by ensemble-averaging the individual field measurements agree well with other measurements. However, the instantaneous velocity fields confirm the existence of instantaneous large-scale structures which are not seen in the DNS results. Also the experiment demonstrates the feasibility of performing PIV measurements in high Reynolds number flows.

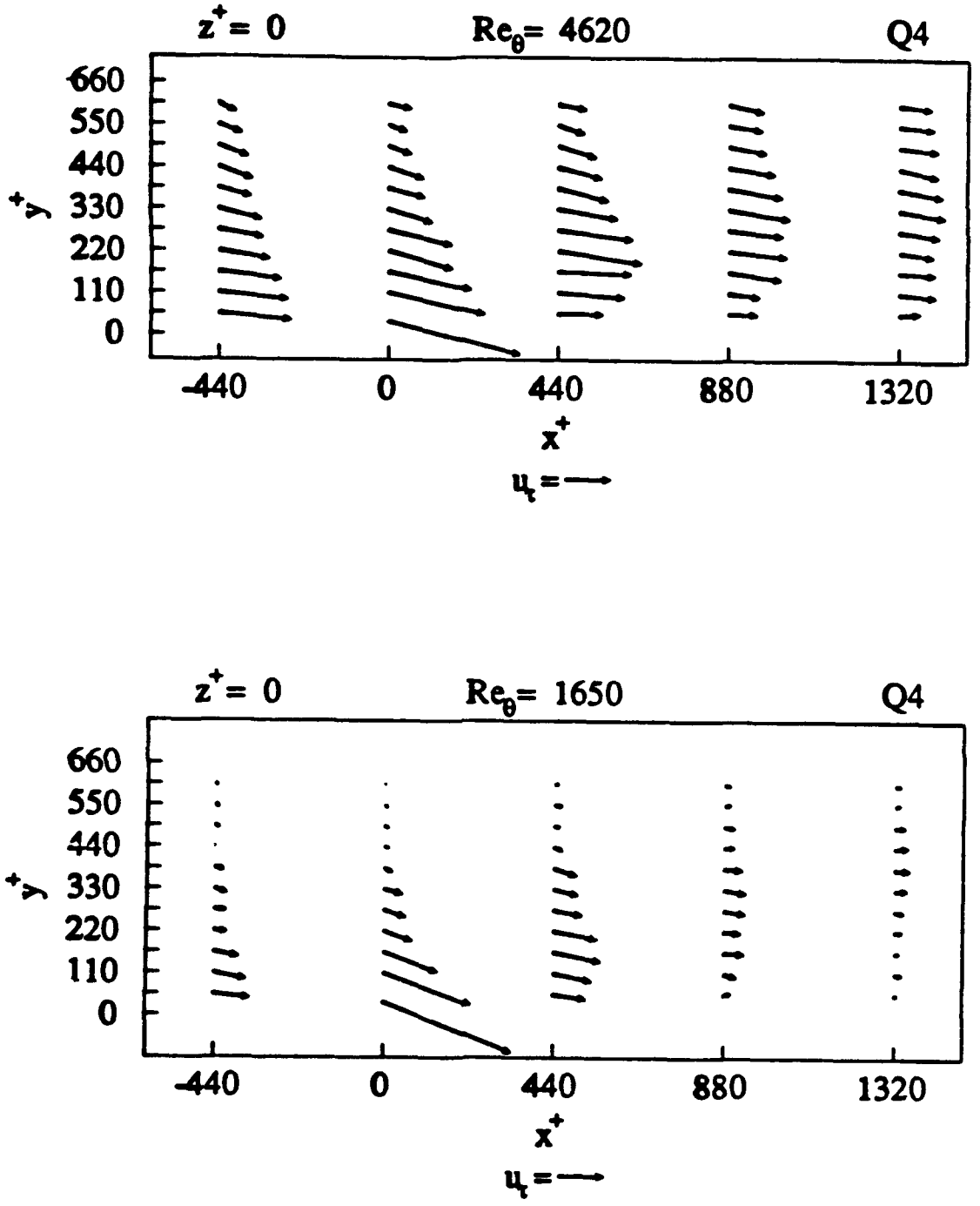


Figure 3. Velocity Vector Maps in the x-y Plane for the Ensemble-Averaged Structure Associated with a Q4 Detection for $Re_\theta$ = 4650 and 1650.

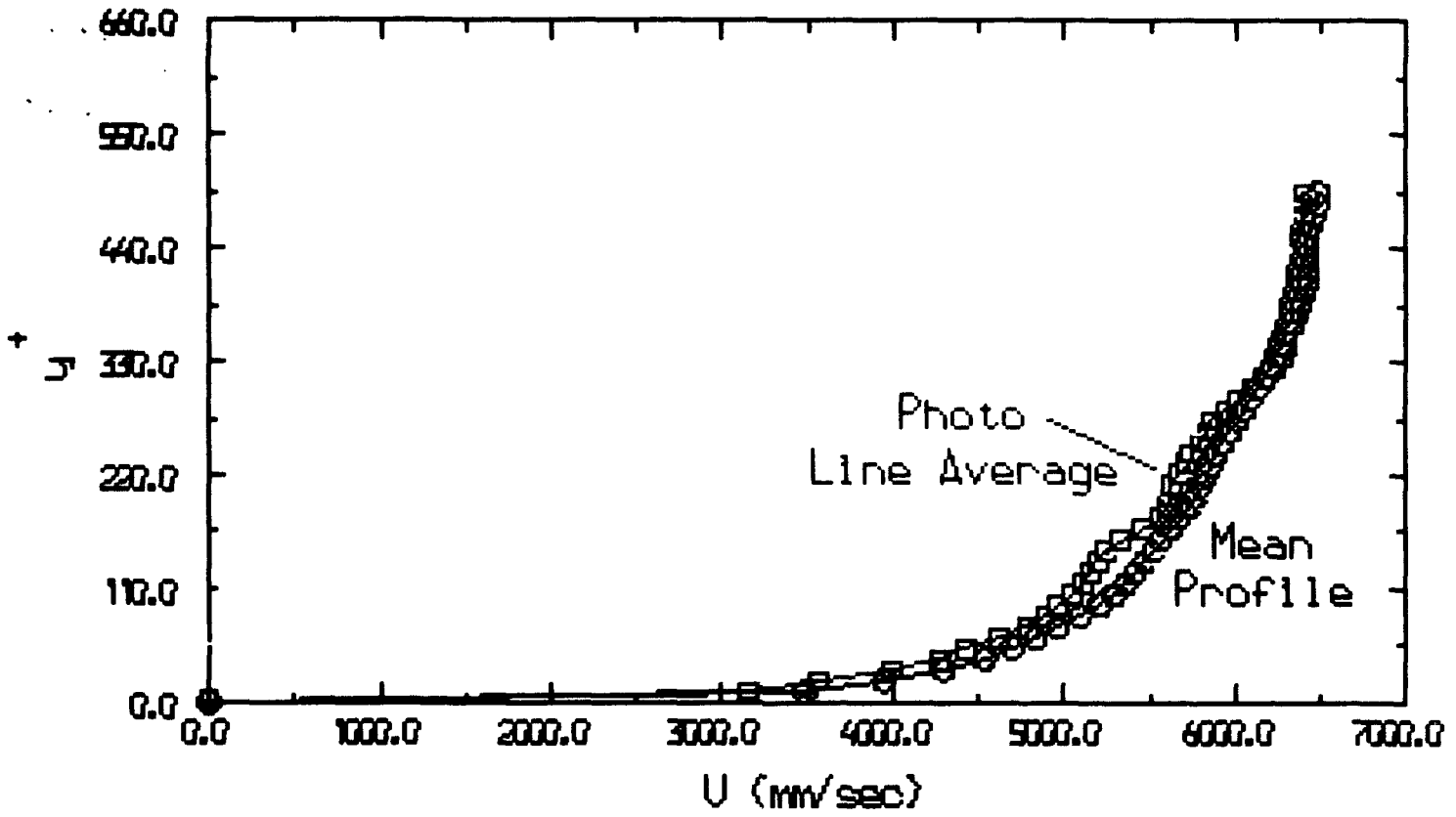


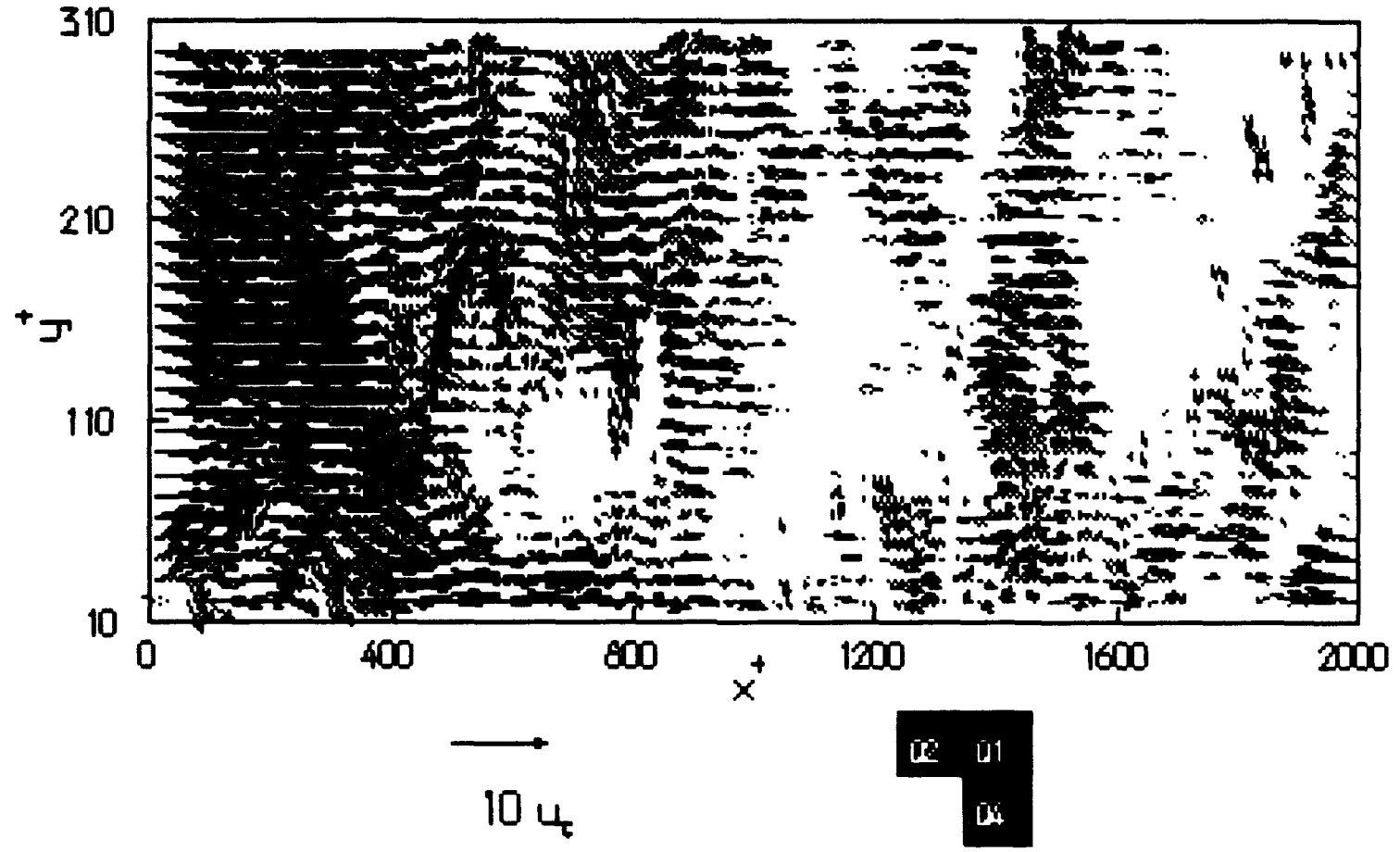


Figure 4. Top:Comparison of Line-Averaged Profile for Bottom Photograph Compared with True mean Profile. Bottom:Quadrant representation For one Photograph.

## III. An Investigation of Wall-Layer Dynamics Using A combined Temporal Filtering and Correlation Technique.

Objectives. Earlier investigations at IIT (e.g., Wark & Nagib (1991) and Naguib & Wark (1992)) indicate that a hierarchy of scales of turbulent motions is associated with the production of Reynolds stress in the wall-layer and that an integral length scale, representative of the hierarchy, scales on the outer length scale (e.g., the momentum ($\theta$) or boundary layer ($\delta$) thickness). Left unanswered were questions regarding the wall (inner)-layer role, and the relative importance of the inner and outer layers in the dynamics of the near-wall region. To answer these questions, Wark et al. (1991) examined the scaling of the conventional spanwise correlation coefficient $R_{\tau u}(z)$ at several heights within the buffer and logarithmic region. They concluded that while outer scaling was successful in collapsing $R_{\tau u}(z)$ in the logarithmic region, a dual-scaling character was observed for the buffer layer (even as close to the wall as $y^+ = 10$) where wall scaling was found to collapse the data for small spanwise offsets and outer scaling was successful for large spanwise offsets.

In this section, the scaling of the spanwise coefficient $R_{\tau u}(z)$ will be further explored in order to understand the lack of wall scaling in the near-wall region. To avoid the indiscriminate integral effect of different types of structures, the correlation coefficient will be determined for narrow band-passed $\tau$ and u signals and their scaling will be examined. If $R_{\tau u}(z)$ for the temporally-filtered signals scale with either wall or outer variables then the dynamics of the turbulent motion(s) within the passed frequency band is, presumably, solely controlled by the wall region or outer layer respectively. If successful, the approach will provide a means of isolating the contribution of outer-layer structures to the turbulent fluctuations from those due to wall-layer structures. Finally, an attempt will be made to assess the contribution and relative importance of outer and inner layer structures to the dynamics of turbulence in the near-wall region.

Results and discussion. Temporal filtering of the time series was implemented using eleven equal-width FIR digital filters spanning the entire turbulence spectrum: the filters were numbered 0 through 10 (Figure 5). Filters # 0, 1 and 2 pass more than 80 % of the energy in the streamwise velocity fluctuations and, hence, discussion will mainly focus on results for these filters. The spanwise correlation coefficient obtained using filter # n will be denoted by ${}_nR_{\tau u}(z)$. Results for the correlation coefficient obtained in the buffer layer using filter # 0 are shown in Figure 6. Figure 6a shows ${}_0R_{\tau u}(z^+)$ obtained at $y^+ = 10$, while Figure 6b shows ${}_0R_{\tau u}(z/\theta)$ results when matching $y/\theta = 0.078$ (corresponding $y^+$ range: 5.5- 17.8) for the different Reynolds numbers. It is clear from the figure that when scaled with inner variables, the correlation results experience a strong Reynolds number dependence. Alternatively, when scaled with outer variables (Figure 6b), the correlation coefficient is much less sensitive to Reynolds number.

Figure 7 represent $R_{\tau u}(z)$ results in the buffer layer when using filter # 1. An excellent collapse of ${}_1R_{\tau u}(z)$ values is obtained at $y^+ = 10$ when z is normalized with

the inner length scale, see Figure 7a. Furthermore, at $y^+ = 10$, the prominent negative correlation peak is depicted from Figure 7a, at $z^+ = 50$: this spanwise location matches the value for one-half the average wave length of the low-speed streaks ($\lambda^+ = 100$) as found by Smith & Metzler (1983), amongst others. Figure 7b demonstrates that the outer length scale fails to collapse the correlation values in the frequency band allowed by filter # 1. For example, as Reynolds number increases the negative correlation peak shifts to lower $z^+$ locations. Though not shown here, inner scaling is found to persist for the remaining filters (#2 through #10). Also scaling results for the logarithmic region are similar to those presented for the buffer layer.

Based on the above results, one can reasonably assume that the contribution of the outer-layer structures to the streamwise velocity fluctuations in the near wall region are confined within the frequency band of filter # 0, whereas, the rest of the u spectrum is dominated by turbulent motions that scale on the viscous length scale. To determine which of these two types of motions is more important, the percentage contribution to the total streamwise fluctuation energy ($\overline{u^2}$) in the near-wall region, due to outer-layer structures (filter #0) and energetic wall-layer eddies (filters #1 & 2), are plotted in Figure 8 at $y^+ = 10$. At low Reynolds numbers most of the u energy is contained in wall-layer eddies; however, as Reynolds number increases, the contribution from the outer-layer structures to ($\overline{u^2}$) increases while the contribution from wall-layer eddies decreases, suggesting that the outer-layer plays a more significant role in wall-layer dynamics as Reynolds number increases.

The results of Figure 8 should however, be viewed with caution. Though the information obtained from Figure 8 indicates that the energy of the outer-layer structures increases with Reynolds number, this does not shed light on the relative role of outer and inner layer structures in relation to the process of Reynolds stress production. To investigate this issue further, a set of x-wire measurements, taken at $y^+ = 35$ for $Re_\theta = 1600$ and 4600, were used to calculate the Reynolds stress ($\overline{uv}$) within the individual frequency bands of filters 0 through 10. The percentage of the total Reynolds stress produced by turbulent motions within each of the frequency bands of the different filters is plotted in Figure 9 for the two different Reynolds numbers. The results from Figure 9 indicate that, independent of Reynolds number, the Reynolds stress production is dominated by wall-layer eddies which produce about 75-80 % of the total Reynolds stress with the eddies in the frequency band of filter # 1 contributing the most to the production process.

Since $R_{\tau u}(z)$ due to turbulent motions with frequencies allowed by filter # 1 produce the negative correlation peak commonly associated with the low-speed streaks, the results from Figure 9 suggest that these streaks, and related turbulent motions are responsible for most of the Reynolds-stress production in the near-wall region. The break-up of low-speed streaks into violent turbulent motions leading to considerable amount of Reynolds-stress production has been known since the early work by Kim et al. (1971). Furthermore, the dominant role of wall-layer structures

in the production of Reynolds stress in the near-wall region agrees with the wall-scaling of the frequency of occurrence of Reynolds-stress-producing events: a generally, but not exclusively accepted result. Evidence of wall scaling of the frequency of occurrence of Reynolds-stress producing events can be found in the work by Blackwelder & Haritonidis (1983) and Luchik & Tiedermann (1986), amongst others.

Conclusions. Using multiple band-pass filters, it was found that structures contributing to the low-frequency range are responsible for the lack of scaling of $R_{\tau u}(z^+)$ and for the disappearance of the "negative dip" (often associated with low-speed streaks) of the spanwise correlation. Moreover, structures contributing to the wall-layer scaling, in the intermediate frequency range, seem to correspond to the low-speed streaks and contain a significant fraction of the energy in the wall-layer turbulent motions.

Investigating the relative role of the individual structures in the dynamics of the near-wall region, it was found that, as Reynolds number increases, the contribution of the outer-layer structures to the streamwise velocity fluctuations increases monotonically: this appears to continue at even higher Reynolds numbers to overwhelm the conventional statistics in the near-wall region. Nevertheless, the Reynolds stress production is dominated by wall-layer structures and outer-layer structures appear to play a minor role in the production process.

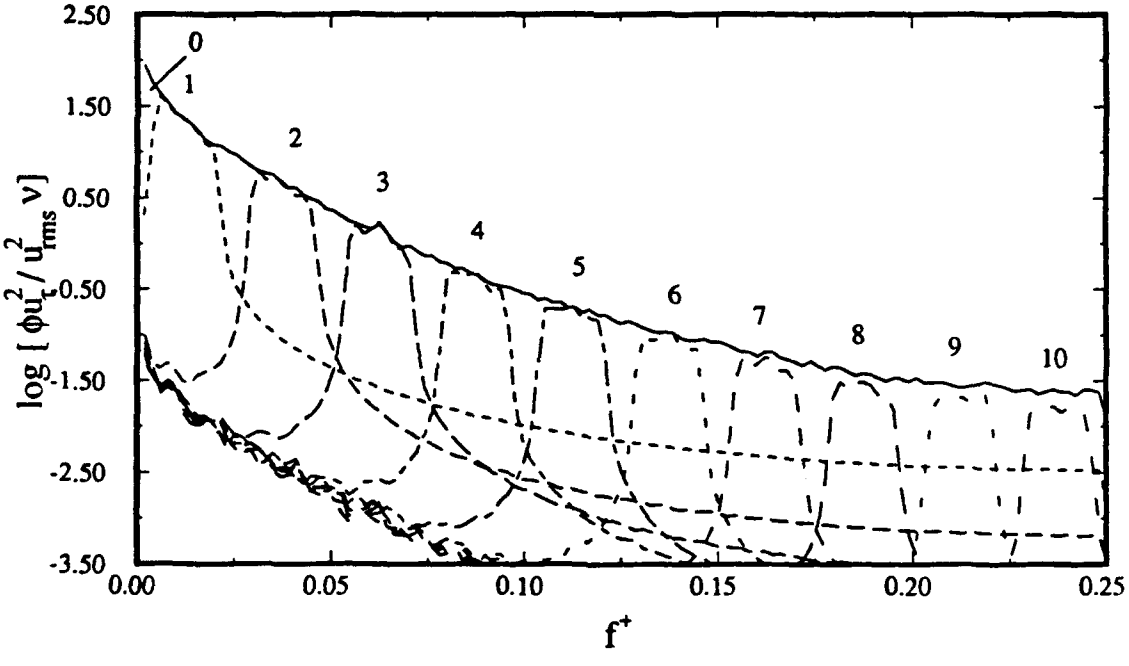


Figure 5. Power spectral density of the unfiltered (solid line) and filtered turbulent signal (for 11 different filters).

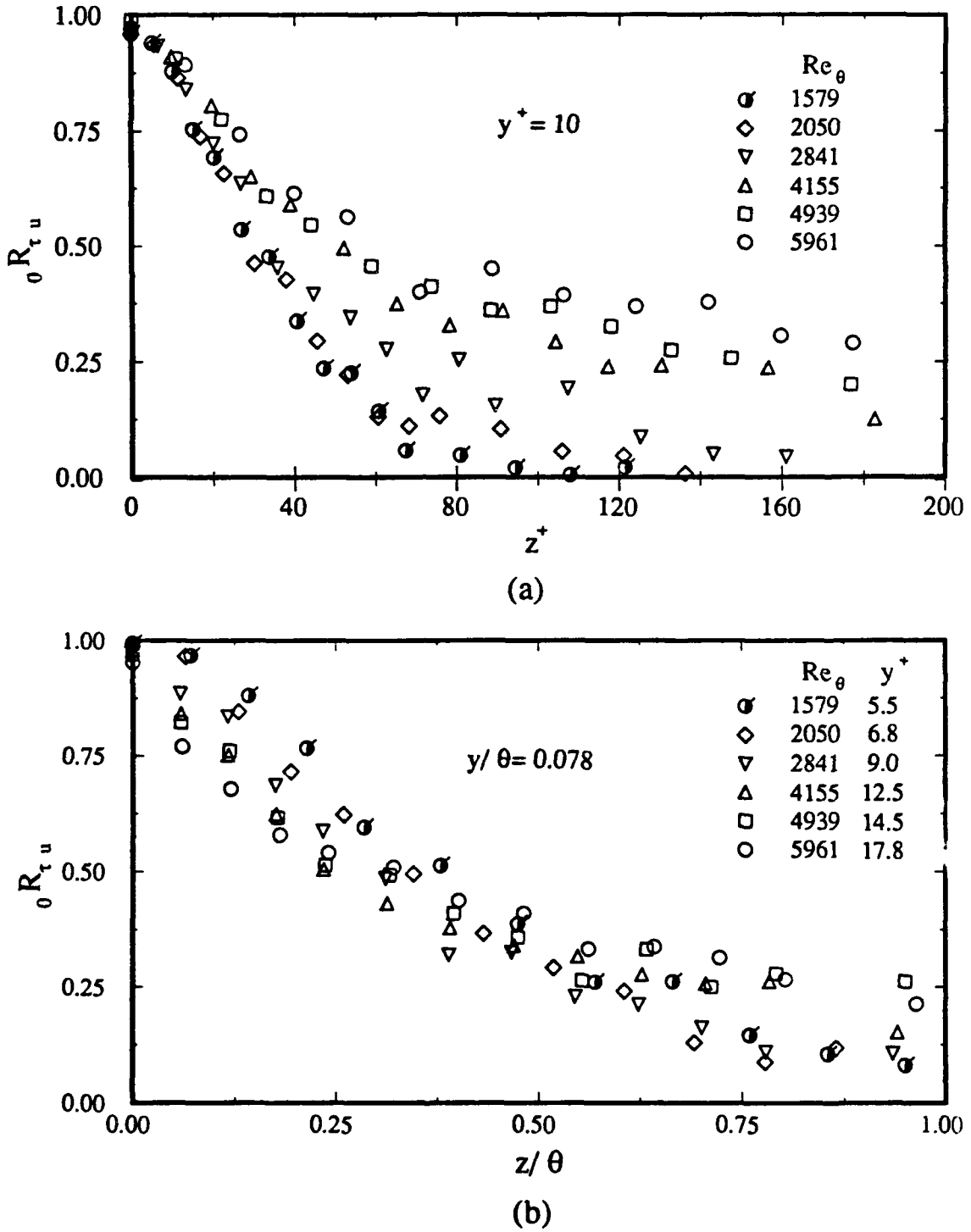


Figure 6. Reynolds number dependence of the spanwise correlation coefficient in the buffer region for the filtered time-series, using filter # 0: a) inner scaling at $y^+ = 10$, and b) outer scaling at $y/\theta = 0.078$.

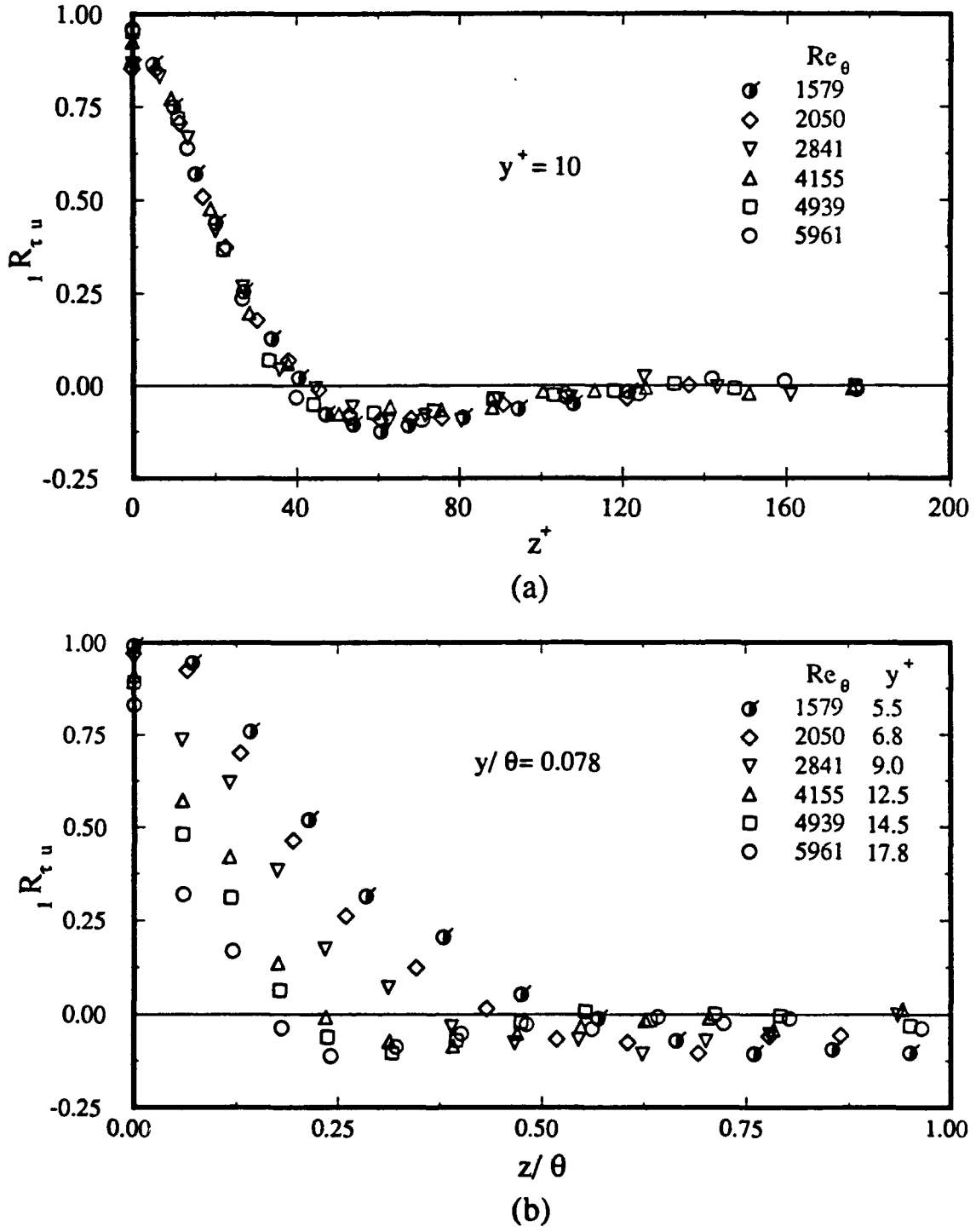


**Figure 7. Reynolds number dependence of the spanwise correlation coefficient in the buffer region for the filtered time-series, using filter # 1: a) inner scaling at $y^+ = 10$, and b) outer scaling at $y/\theta = 0.078$.**

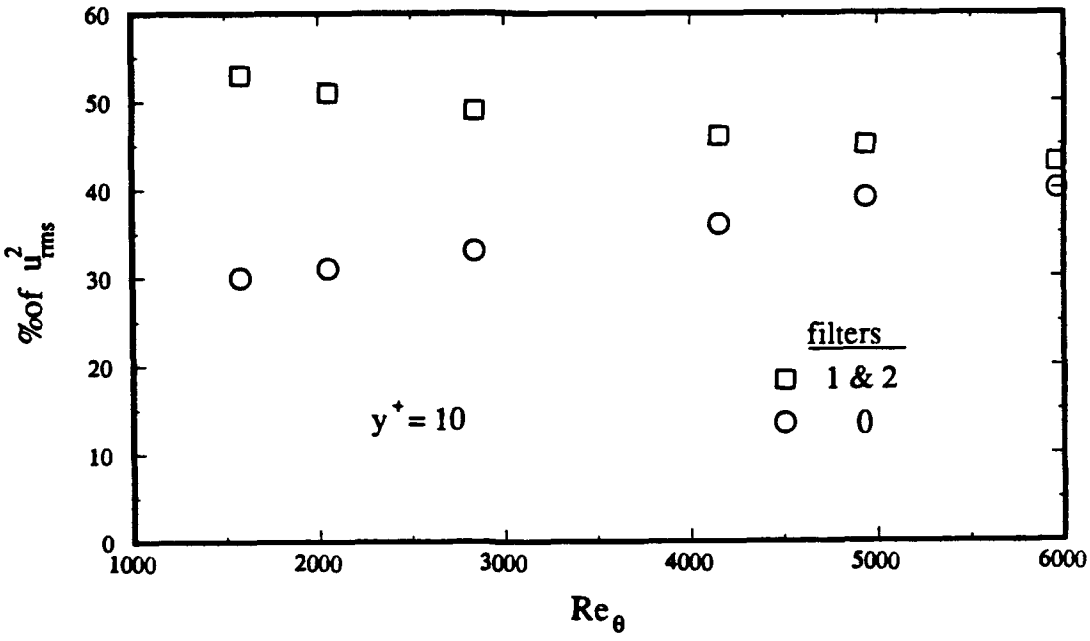


Figure 8. Comparison between the contribution of outer-layer structures and energetic wall-layer events to the energy in the streamwise velocity fluctuations, for $1579 \leq Re_\theta \leq 5961$.

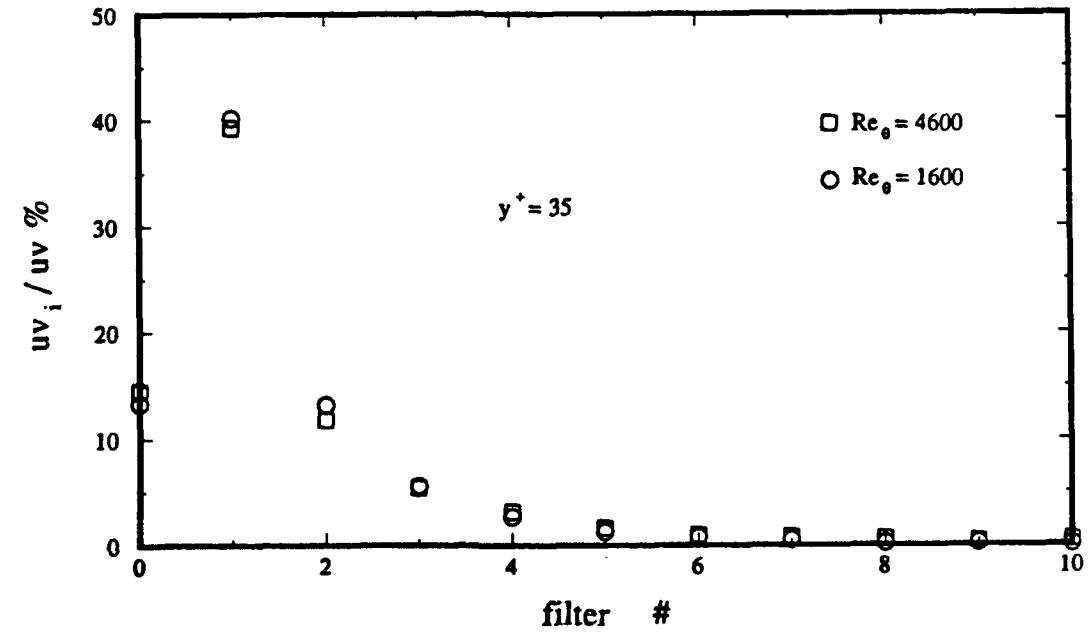


Figure 9. Relative contribution to Reynolds stress production at $y^+ = 35$ due to band-pass filtered u and v signals, using filters # 0 thru 10, for $Re_\theta = 1600$ & 4600.

## IV. Effects of Transition and Outer-Layer Intermittency on the Reynolds-Stress Producing Events in a Turbulent Boundary Layer

Objectives. The present study was conducted to determine the relation between the outer-layer intermittency and the wall layer turbulent production process. This investigation was performed in a zero pressure gradient turbulent boundary layer at $Re_\theta = 4942$.

Experimental Procedure. Data was acquired with a X-wire probe which was traversed at various heights ($y/\delta$ = 0.4 to 1.5 in steps of 0.1) to detect the interface between turbulent and non-turbulent fluid, while a shear-wire probe was kept at $y^+ = 0$, and a single-wire was placed at one of four $y^+$ positions ($y^+$ = 10, 15, 30 and 55). The three probes were placed at the same streamwise location and the X-wire intermittency probe was placed at both $\Delta z^+ = 0$ and $\Delta z^+ = 80$ which respect to the single u-wire and shear-wire probes.

Results. Various statistical measures on the time series acquired by the shear-wire and single u-wire probes were determined when the X-wire intermittency detector probe encountered either turbulent or non-turbulent fluid. Conditional averages and probability density functions of the streamwise component of the wall shear-stress and streamwise velocity fluctuation normalized by their root mean square values ($u/u_{rms}$ and $\tau/\tau_{rms}$) were obtained. Furthermore, the conditional U-level and shear-stress detected events were obtained to examine the effect of the outer-layer intermittency on the wall-layer turbulence production process.

The intermittency detector scheme employed in the present investigation is given by Hedley and Keffer (1974): this scheme is based on both the streamwise and normal components of velocity. A criterion function, $S(t_j)$, given by

$$S(t_j) = \frac{\Delta T^2}{1 + \frac{T_s}{\Delta T}} \sum_{i=j-\frac{T_s}{2\Delta T}}^{i=j+\frac{T_s}{2\Delta T}} \left\{ \left[\frac{\Delta u}{\Delta T}\right]^2 + \left[\frac{\Delta v}{\Delta T}\right]^2 \right\}_i$$

was used to detect the turbulent/non-turbulent interface: $\Delta T$ is equal to 1/(acquisition frequency) and is 1.5e-04 sec and a non-dimensional hold time, $T_s/2\Delta T$, equal to two was used in this investigation.

An adjustable threshold level C equal to 0.1 was chosen to threshold the criterion function (S) such that the intermittency level at 0.8 $y/\delta$ was approximately 50%. This value of 50% for 0.8 $y/\delta$ is taken from the discussion of Kovasznay et al. (1970) and Corrsin and Kistler (1955). The resulting function is called an indicator or intermittency function which is a random square wave with values of unity for turbulence and zero otherwise. This function was subsequently used to condition

the signals from the single and shear-wire probes to study the effect of the outer-layer intermittency on wall-layer Reynolds-stress producing events.

The intermittency factor $\gamma$ or $\overline{I}$ is then defined as the time-averaged value of the intermittency function $I(t_j)$: $\gamma = \overline{I} = \sum_{i=1}^{N} \frac{I(t_i)}{N}$ where N is the number of points in the time series.

The variation of the intermittency factor ($\gamma$) across the boundary layer varies smoothly from values of unity deep in the boundary layer to zero outside of the boundary layer. The profile matches the results by Kovasznay et al. (1970), Hedley and Keffer (1974) and Guezennec and Nagib (1990).

If we let $Q(t_j)$ represent an arbitrary time series, the *conventional* and *conditional* time average of $Q(t_j)$ when the intermittency detector has a value of one (often called a turbulent bulge) and zero (non-turbulent conditions) is given by:

$$\overline{Q} = \sum_{j=1}^{N} \frac{Q(t_j)}{N} \qquad Q_1 = \sum_{j=1}^{N} \left[ \frac{I(t_j)Q(t_j)}{N\overline{I}} \right] \qquad Q_0 = \sum_{j=1}^{N} \left[ \frac{[1-I(t_j)]Q(t_j)}{N\left[1-\overline{I}\right]} \right]$$

respectively. It then follows that $\overline{Q} = \gamma Q_0 + (1-\gamma)Q_1$.

The conditional probability distributions of $u/u_{rms}$ are shown in Figure 10. The top plot represents the turbulent conditional zone average; whereas, the non-turbulent conditional zone average is given in the bottom plot. Only results for $u/u_{rms}$ at $y^+ = 10$ is shown here: the results for $\tau/\tau_{rms}$ and for $u/u_{rms}$ at $y^+ = 15$, 30 and 50 are similar to those for $y^+ = 10$. The streamwise and spanwise offsets between the intermittency detector probe and streamwise velocity probe was $x^+ = 0$ and $z^+ = 0$ as given in the plots.

Blackwelder and Kovasznay (1972) obtained point averages of the streamwise velocity component as a function of the distance from the intermittency detector probe. The point averages of the streamwise velocity fluctuations at the "fronts" and "backs" of the turbulent bulge were found to be significantly different. The "front" of a turbulent bulge is defined as the location at which the probe detects a non-turbulent/turbulent interface; likewise, the "back" is the location where the probe detects a turbulent/non-turbulent interface. Based upon their results the present data was processed to determine the conditional zone averages upon detection of the "fronts" and "backs" of the turbulent bulges. Figure 11 depicts the conditional averages for $u/u_{rms}$. The conditional averages for the "fronts" and the "backs" are seen in the top and bottom plots respectively.

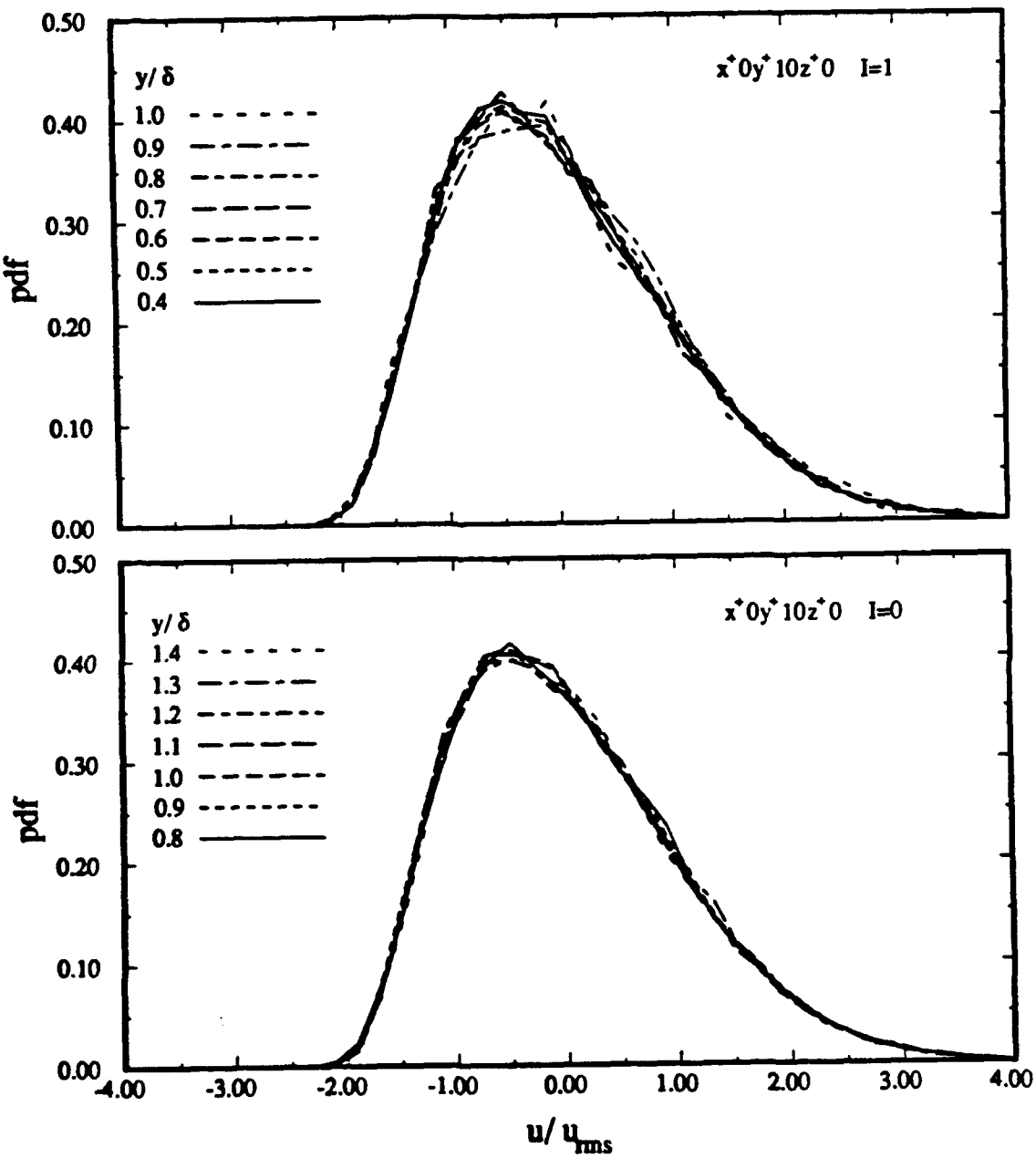


Figure 10. Comparison of Conditional Probability Density Functions of $u/u_{rms}$ at $y^+ = 10$, for I = 1 and 0, at several y/d Intermittency Detector Positions.

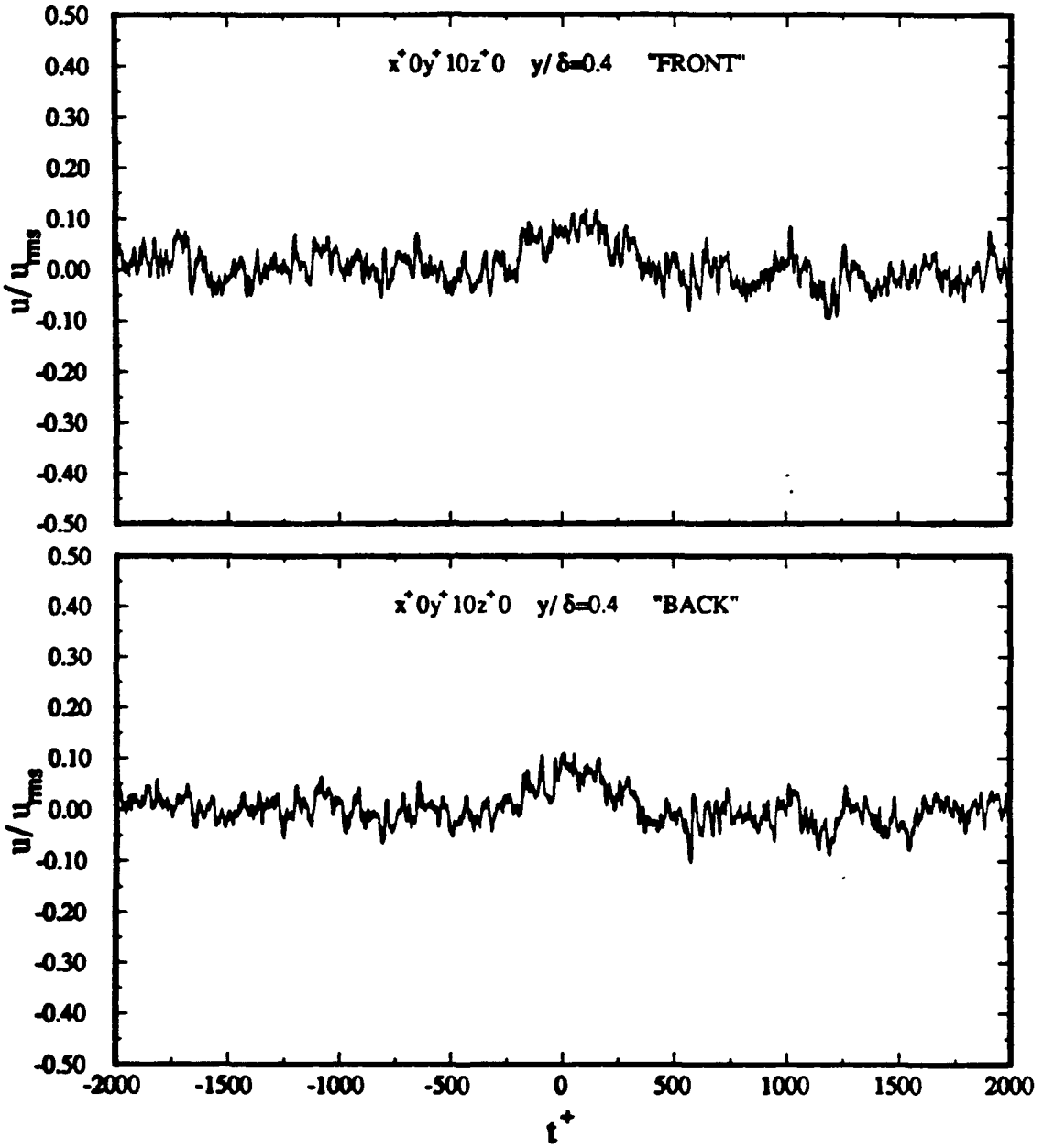


Figure 11. Comparison of Conditional Zone Averages of $u/u_{rms}$ at $y^+ = 10$, for the "fronts" and "backs" of Turbulent Bulges, as a function of $t^+$ for several y/d Intermittency Detector Positions.

In addition, further processing to determine what effect, if any, the turbulent bulges have upon the Reynolds-stress producing events as detected by the U-level detection scheme from Lu and Willmarth (1973). The U-level detected events were counted either when the intermittency function (I) indicated turbulent or non-turbulent fluid. Normalized by the time duration of the turbulent bulge ($T_\gamma$) or non-turbulent regions ($T_{1-\gamma}$) for the two conditions I = 1 and 0 respectively, the number of U-level detected events can be seen in Figure 12.

Concluding Remarks. Even though the influence of the outer-layer on the wall-layer has been documented, the results presented above suggest that the intermittent character of the outer flow in a turbulent boundary layer is not responsible for this influence. This is consistent with turbulent channel and pipe flow studies in the sense that the wall-layer statistics are remarkably similar between these three turbulent wall-bounded shear flows; yet, turbulent channel and pipe flow do not exhibit the same intermittent character as a turbulent boundary layer.

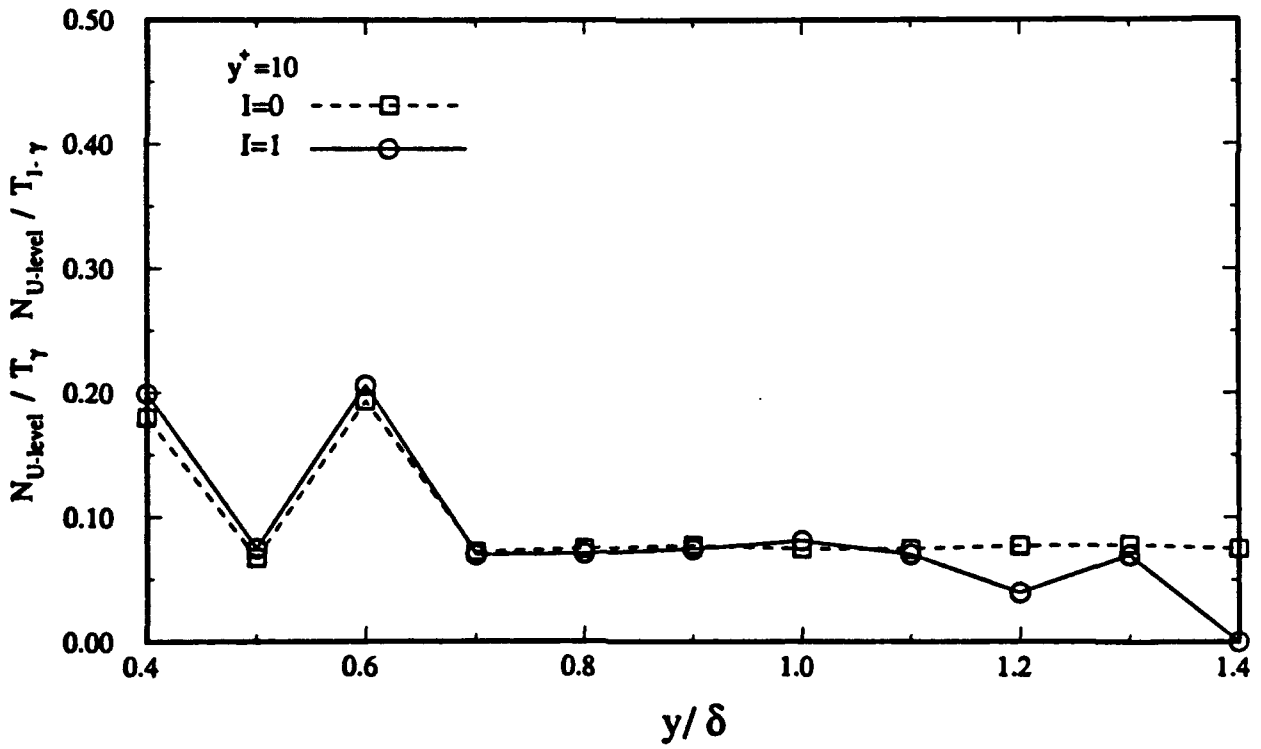


Figure 12. Comparison of Number of U-level Detected Events at $y^+ = 10$, for I = 1 and 0 as a function of Intermittency Detector Location.

## V. Visualization of Dynamically Active Events in a Turbulent Boundary Layer

Summary. Two- and three-dimensional views of the turbulence in the wall region of a turbulent boundary layer were recorded on high speed film with the aid of locally introduced multiple smoke sheets and several laser-light planes. The simultaneous acquisition of the wall-shear signal at an $Re_\theta$ of 2100 allowed the identification and analysis of the instantaneous coherent structures associated with turbulence production. Information on the character, size, location, intensity and duration of these structures was cataloged and in most cases statistics were derived from them. The analysis of the visual records was carried out in the frame of a conjectured model which is based on extensions of Theodorsen's (1952) original hairpin vortex flow module.

The observed structures are consistent with a model based on the hairpin vortex, and reveal at least as many pairs of counter rotating legs (symmetric vortices) as there are ones appearing as one longitudinal vortex (asymmetric hairpins). The high and low wall shear detection of these vortices appears to identify the outside edge of them and their plane of symmetry, respectively. A great number of these vortices are of such short duration that it is easy to confuse them with the axisymmetric mushroom-type structure or typical eddy. However, many of them can be quite long on the order of 900 $x^+$, which is consistent with the experimental results of Naguib and Wark (1992) and Wark and Nagib (1991) and the processing of numerical data by Robinson (1991).

These dynamically-active structures have normal velocities exceeding 18% of the local mean and reach from the wall to elevations well beyond 200 $y^+$. Their average transverse spacing is proportional to the height they are identified at, and the more energetic ones are spaced farther apart from each other in the spanwise direction. The probability density distribution of their sizes and duration times are supportive of a broad hierarchy of scales, as discussed by Wark and Nagib (1991), even at the present relatively low Reynolds number. Finally, while the data do not conclusively confirm the merging of vortices model by Wark and Nagib (1989) as an important mechanism of their growth, as many as 5 to 10% of the identified structures may have participated in such vortical connection.

Objectives. Over the past decade, the turbulent boundary layer group at IIT has focused on the problem of revealing the character and kinematics of large scale coherent motions associated with the production of turbulence in the wall layer. The earlier results, based on extensive velocity data over a three-dimensional grid in space, revealed the existence of ensemble-averaged structures associated with the production of turbulence. As with any ensemble-averaged result, questions arose as to the instantaneous nature of these structures. The more recent work has focused on the nature of the instantaneous structures. The focus of the present investigation is also to reveal the instantaneous dynamics of these structures by using flow visualization combined with a non-obtrusive detection probe (Guezennec, 1985) to identify and characterize the individual turbulence producing events. To aid in

deciphering the films, a model, based on the hairpin vortex, is conjectured to be the dominant structure responsible for turbulence production in the boundary layer. Various two and three dimensional views of the visualizations are examined to find evidence that is in support of the model; see Figures 13 and 14.

In the course of the investigation, a new technique for analyzing the visualization films was developed which allowed for the investigation of the spanwise spacings at which these structures occur. Using this new technique, the effects of hemispherical artificial disturbances placed at the wall on the turbulence producing structures were also examined.

Evidence of the Hairpin Vortex Structure. Several investigators have proposed the hairpin vortex as the basic flow module responsible for the production of the turbulent kinetic energy, and for sustaining the turbulence, in boundary layer flows. First introduced by Theodorsen (1952), the hairpin vortex consists of two counter rotating streamwise vortices near the wall, connected through an inclined neck to a transverse vortex away from the wall called the head. The hairpin vortex is a good choice for a turbulent model because of the Reynolds-stress production associated with it. By pumping low momentum fluid up away from the wall in the middle (Q2 or ejection event), and pushing high momentum fluid down toward the wall on the sides (Q4 or sweep event), the hairpin vortex is generating the cross-gradient mixing necessary for the production of turbulent kinetic energy.

Many investigators have isolated components of the hairpin vortex, such as the streamwise vortices or the spanwise vortices forming the head, and have conjectured as to their relation with the hairpin vortex, but have failed to provide substantial evidence linking all of the hairpin vortex components together in a fully turbulent boundary layer. Using simultaneous views of the of the x-y and y-z planes in the Bi-Plane set up, Figure 14, it was hoped that the connection between the transverse vortices, seen as the curling over of ejected spindles of smoke, and the lifted streamwise vortices, seen as mushroom shapes in the spanwise view, would become apparent. However, due to the scarcity of smoke in the higher regions, and the difficulty in marking only the hairpin vortex element, this connection was never consistently made. It was noted that when fluid was violently ejected from the wall that large bulges of smoke appeared in the x-y plane after the ejection passed through. This could indicate the presence of the counter rotating legs of the hairpin vortex, pushing the smoke up in the middle.

The analysis of the high-speed visualization records, in connection with the wall-shear signals, revealed several cases after a T- detection with an arch-like structure appearing in the y-z plane centered about the plane of detection. In the case of T+ detection, the arch-like structure appeared to one side or on both sides of the central plane. However, due to the difficulty in examining the patterns in the y-z plane of the Bi-Plane configuration, the spanwise details of the bulges were unclear.

More detailed information on the streamwise vortices was found in the Z-Type and 3Z-Type films, recorded using the arrangements of Figure 13. In both of these film types, a variety of mushroom shapes and question mark-like shapes appeared

very often, signifying streamwise vortices. The 3Z-Type films also allowed for the investigation of the evolution of the structures as they passed through successive light sheets. Several progressions of structures passing through the sheets were traced onto grids. These tracings presented clear evidence of streamwise circulation between planes due to counter rotating vortices.

The evidence described above, of counter rotating vortices, transverse vortices, and so on, confirms that there are smoke patterns occurring, associated with the production of turbulence as detected by the shear-wire probe, which essentially support the existence of the hairpin vortex structure. The extent to which these structures occur is still unknown, and the exact connection between the streamwise vortices and the spanwise vortices is still somewhat unclear. To further test the relation of the structures to T+ and T- events, the structures appearing in the Z-Type films were correlated with the shear-stress events.

The correlation results indicate that T+ detections are associated with structures occurring farther away from the detection point. This is in support of the model since T- events should correspond to structures going over the top of the probe while T+ events should correspond to structures passing to the side of the probe. The results also indicate that the average spacing between successive structures occurring about the probe is larger for T+ associated structures than otherwise. This may indicate that the structures causing the strong T+ events are larger as they occur at larger spanwise spacings.

Similar results were found in the direct numerical simulation results of Spalart (1988), by Robinson (1991). He identified vortices by their elongated low pressure cores, and found that streamwise vortices near the wall are sometimes connected to a transverse vortex forming either a symmetric or an asymmetric hairpin vortex. These vortical structures were associated with Q2 or ejection events, on the upward rotating sides of the streamwise vortices, and Q4 or sweep events, on the outside downward rotating sides of the streamwise vortices. If such events were marked with smoke near the wall, and the resulting patterns were observed at relatively short distance downstream, as with in the Z-Type set up, Q2 events would appear as mushroom shapes or bulges of lifted smoke, while Q4 events would be associated with the absence of smoke and the existence of structures to the side. By finding that the T+ events are associated with ejection structures occurring farther away from the probe than on the average, the hairpin model is supported. The results also indicated that the T+ detection is more likely to be associated with one vortex passing to one side rather than two similar ones on each side of the wall probe.

In summary, structures associated with the production of turbulence were found to have characteristics consistent with the hairpin vortex model. However, no consistent evidence is available of the fact that the streamwise and transverse vortices have to be a part of the same structure (the hairpin vortex) responsible for the production. Furthermore, a correlation was found between T+ events and structures occurring at larger spacings farther away from the detection probe, which is supportive of the model.

Spanwise Occurrence of Dynamically Active Events. The low speed streaks have been documented most extensively by Smith and Metzler (1983) who showed that the spanwise mean streak spacing of 100 $z^+$ is invariant over a wide range of Reynolds numbers. Kim et al. (1971) among others, found that the low speed streaks would lift away from the wall, oscillating, then breaking down and causing the violent ejections of low speed fluid away from the wall. This process, called bursting, was found to contribute to a large fraction of the turbulent kinetic energy found in a turbulent boundary layer. Several studies were conducted in an attempt to find the cause and characteristics of this low speed streak lift up and busting process.

Several probe based detection techniques were also developed to identify a burst, and were used to find the characteristics of the bursts, such as the bursting frequency, the conditionally averaged flow field associated with a burst, and so on. Recently, Antonia and Bisset (1990) used an array of hot wires aligned in the spanwise direction to obtain the spanwise contours of the conditionally averaged streamwise velocity signature based on detections of bursts. These data gave information on the spanwise extent of singly occurring bursts, but not on the spanwise separation between different bursts.

Other investigations dealing with the bursting event reveal information on the characteristics of single burst events, their relation to sweep events, or their rate of occurrence at a single streamwise station. None of these investigations deal with the relative spanwise occurrence or separation between these burst events. Similar observations can be made about the documentation of any of the features associated with strong production of Reynolds stresses in wall bounded flows.

In this investigation a technique has been developed which addresses the question of spanwise spacing and interaction between successive spanwise turbulence producing events and structures. The technique basically involves introducing smoke into the flow, using smoke wires parallel and near to the floor, and looking for vertical excursions of the smoke illuminated by a laser-light sheet oriented in the y-z plane and located 1100 $x^+$ downstream from the smoke wires. The vertical excursions of smoke seen in the films are referred to as ejection type structures whose strength is based on what threshold height they reach in the images; see Figure 15. The spanwise locations of such events are recorded for every forth frame in a high speed film. From these data the spacings between the structures as well as the structures duration in time can be investigated.

For this procedure the Z-Type film set up is used and both plain and artificially disturbed cases were examined. Some of the films had a high smoke wire configuration, where both sweep and ejection events could be identified. By following the structures from frame to frame, it became evident that some structures lasted for significant periods of time. Figure 16 shows the probability- density histograms for the length of the structures. The plots indicate that the most probable duration of a structure is less than a $t^+ = 6$, and that the mean duration ranges between 18 $t^+$ and 22 $t^+$ for the various plain and undisturbed cases. If these structures are linked to counter rotating vortices lifting up the smoke in the middle

of the structure, then these results would indicate that these vortices can be quite long, on the order of 900 $x^+$ (based on a convection speed of the mean velocity at a $y^+$ of 60), but are typically on the order of 300 $x^+$ units. This is in agreement with IIT's earlier experiments (Wark and Nagib, 1991, and Naguib and Wark, 1992) and with the direct numerical simulation data analyzed by Robinson (1991), where he found that typical legs trailing from hairpin-like vortices were on the order of 400 $x^+$ long.

The second facet of these events discussed is the spanwise spacing at which these events occur. Here the structures were identified using three different thresholds. For each threshold the structures were located in each frame and the spacing between two adjacent structures was calculated for every structure pair of that threshold in a film. The resulting statistics for the spacings are listed in Table 1, and some of them are plotted in Figure 17. The results indicate that the two plain cases show good repeatability including the standard deviation.

These dynamically-active structures have been identified to have normal velocities from 6 to 18 % of the local men velocity and to reach elevations well above 200 $y^+$ for the present $Re_\theta$ of 2080. The mean transverse spacing of these vertical structures is proportional to the height at which they are identified, with the more energetic structures more widely separated. The higher the elevation these structures are marked the wider their mean spacing appears to be in wall units, although this increase does not seem to be linear. The probability density functions of the spacing of these structures is strongly supportive of the hierarchy of scales for these dynamically active events as discussed by Wark and Nagib (1991) and Naguib and Wark (1992).

The last two films were of the high smoke wire type where both sweep and ejection type events were examined. Here only threshold one and two were available due to the limited number of structures appearing in these films. The PDF's for the threshold one case of sweeps and ejections is shown in Figure 17. The results in the case of one film confirm the hypothesis that the ejection events coming from the wall are stronger and larger than the sweep events going down towards the wall.

In summary, a new technique was developed where the spanwise occurrence of dynamically active events is investigated. Several characteristics of these structures have been revealed through this type of procedure. Finally, the effects of the present form of artificial disturbances were found to be minimal, and it is difficult to speculate as to their relation to the ejection events, beyond statements made in the previous section.

Table 1. Statistics of Spanwise Structure Spacing

| Film: | Smoke wire heights (cm) | Thresh-hold | Number of structure pairs | Mean spacing $\lambda^+$ | Std. dev. $\sigma^+$ | Mean spacing $\lambda^+ / dy^+$ | Mean spacing $\lambda^+ / h^+$ |
|---|---|---|---|---|---|---|---|
| 1: Control case (ejections) | 0.25, 0.50 | 1 | 926 | 308 | 155 | 4.50 | 2.25 |
| | | 2 | 678 | 354 | 170 | 3.44 | 2.08 |
| | | 3 | 243 | 437 | 187 | 3.19 | 2.13 |
| 2: Control case (ejections) | 0.25, 0.50 | 1 | 854 | 315 | 152 | 4.60 | 2.30 |
| | | 2 | 490 | 371 | 174 | 3.61 | 2.17 |
| | | 3 | 100 | 463 | 210 | 3.38 | 2.25 |
| 3: Bumps at $x^+ = 400^*$ (ejections) | 0.25, 0.50 | 1 | 615 | 343 | 174 | 5.00 | 2.50 |
| | | 2 | 412 | 384 | 198 | 3.74 | 2.24 |
| | | 3 | 68 | 499 | 230 | 3.64 | 2.43 |
| 4: Bumps at $x^+ = 800^*$ (ejections) | 0.25, 0.50 | 1 | 609 | 341 | 161 | 4.98 | 2.49 |
| | | 2 | 449 | 375 | 173 | 3.65 | 2.18 |
| | | 3 | 115 | 462 | 200 | 3.37 | 2.25 |
| 5: Ejections | 1.90, 2.15 | 1 | 119 | 402 | 203 | 5.87 | 1.11 |
| | | 2 | 43 | 456 | 203 | 4.43 | 1.15 |
| Sweeps | 1.90, 2.15 | 1 | 138 | 381 | 215 | 5.56 | 1.97 |
| | | 2 | 48 | 378 | 199 | 3.71 | 2.40 |
| 6: Ejections | 2.35, 2.60 | 1 | 79 | 370 | 235 | 5.40 | 0.87 |
| | | 2 | 21 | 454 | 236 | 4.42 | 0.99 |
| Sweeps | 2.35, 2.60 | 1 | 296 | 336 | 184 | 4.91 | 1.75 |
| | | 2 | 118 | 413 | 209 | 4.02 | 2.62 |

* Indicates the distance from the laser-light sheet to the row of bumps.

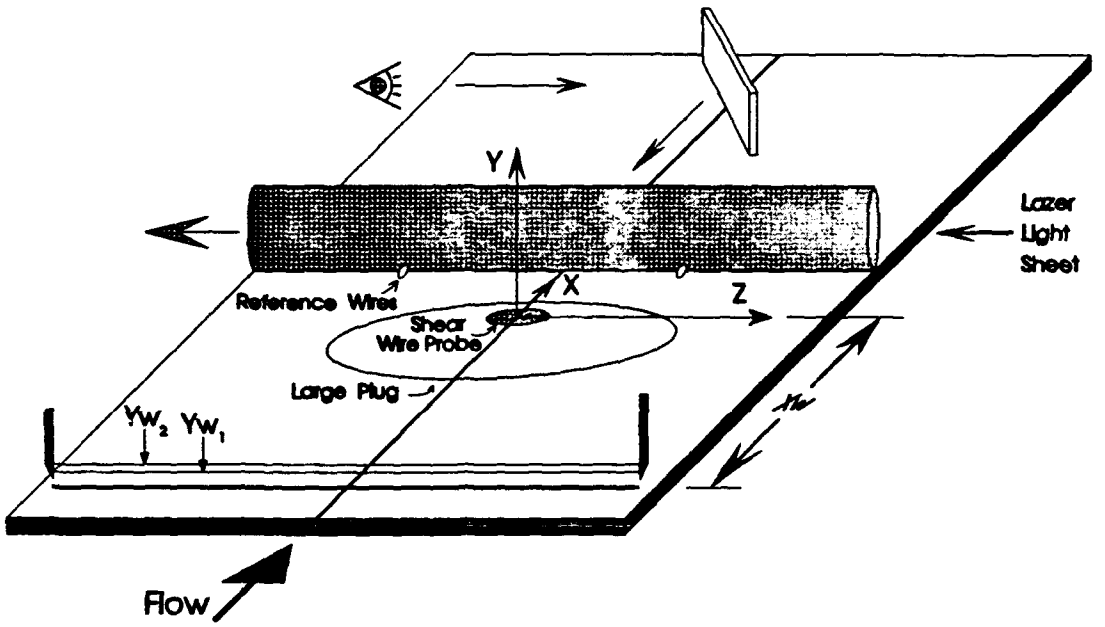


Figure 13a Schematic of Laser-Light Sheets Arrangement for Z-Type Visualization Set Up

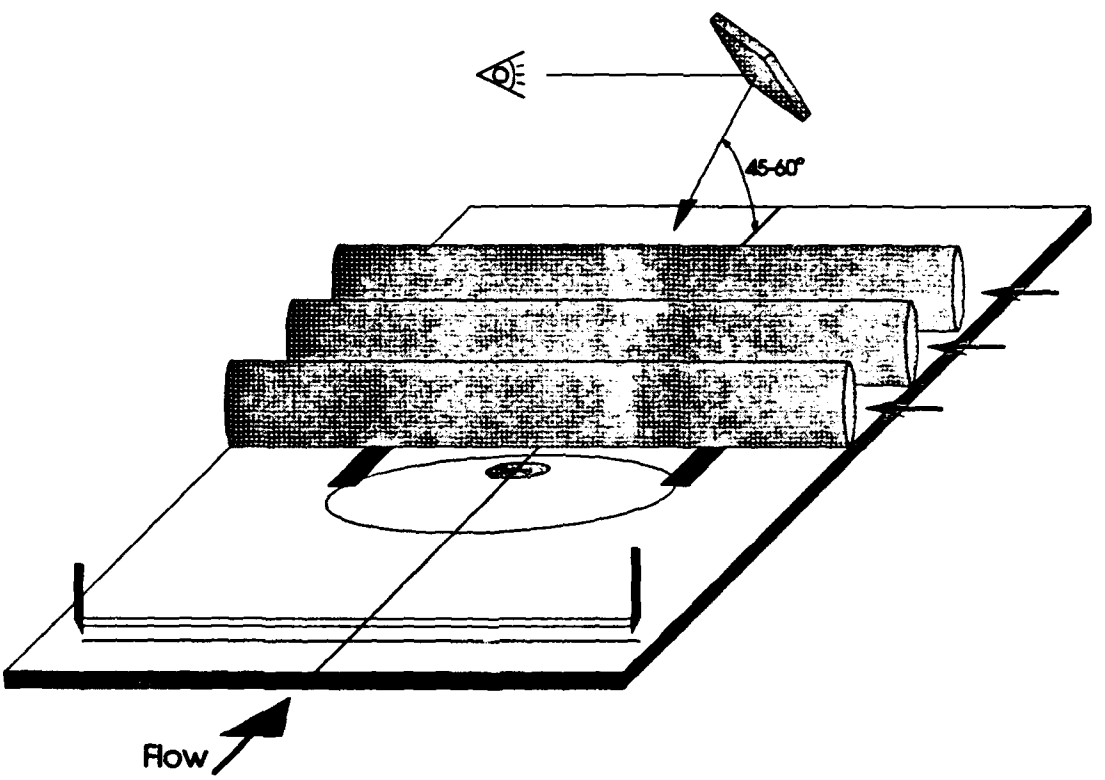


Figure 13b Schematic of Laser-Light Sheets Arrangement for 3Z-Type Visualization Set Up

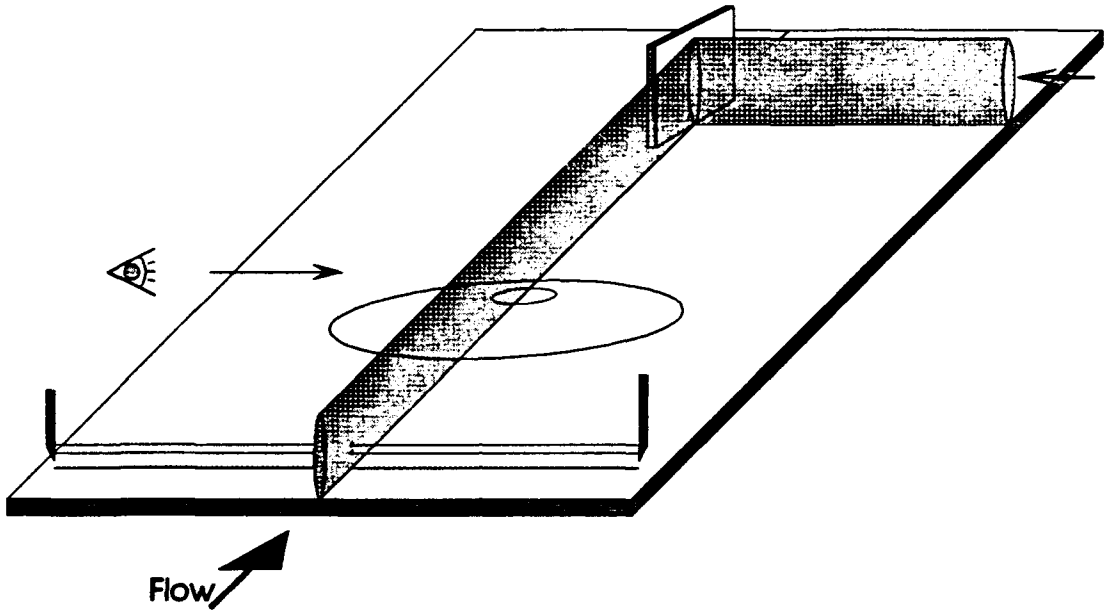


Figure 14a Schematic of Laser-Light Sheets Arrangement for X-Type Visualization Set Up

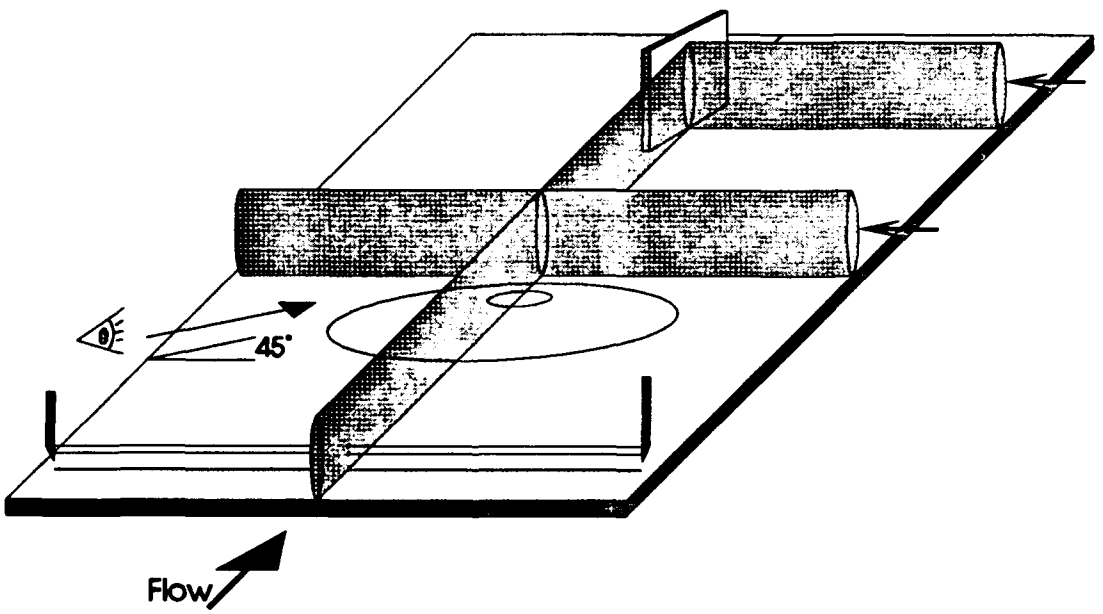


Figure 14b Schematic of Laser-Light Sheets Arrangement for Bi-Plane Visualization Set Up

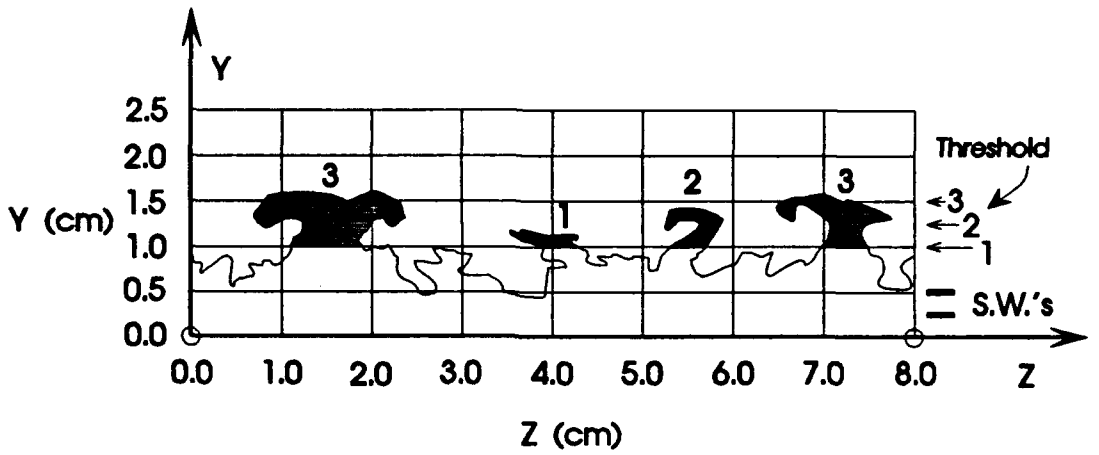


Figure 15a Typical Trace Plot of a Low Smoke Wire Z-Type Image

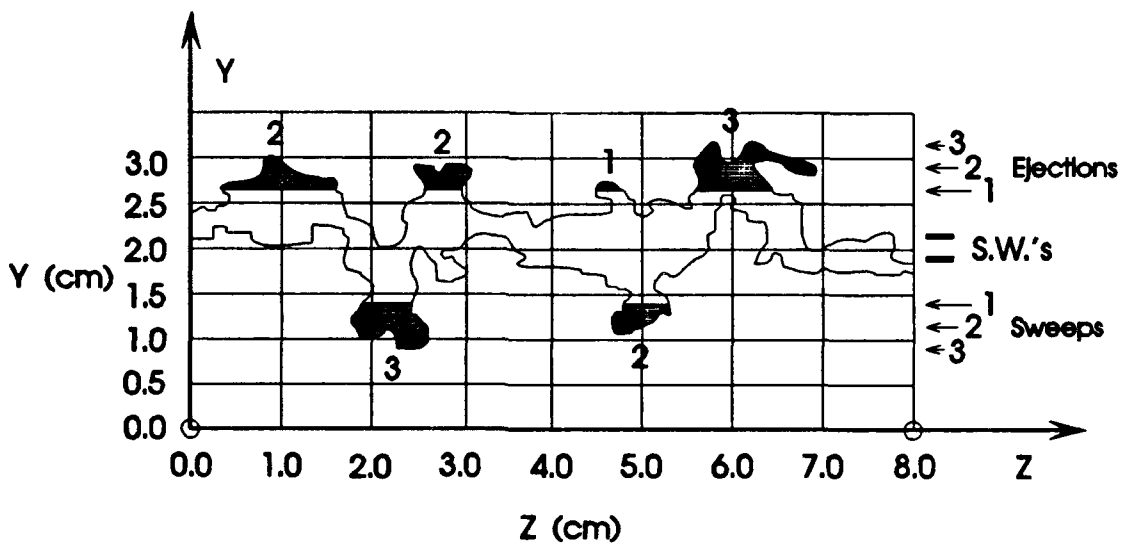


Figure 15b Typical Trace Plot of a High Smoke Wire Z-Type Image

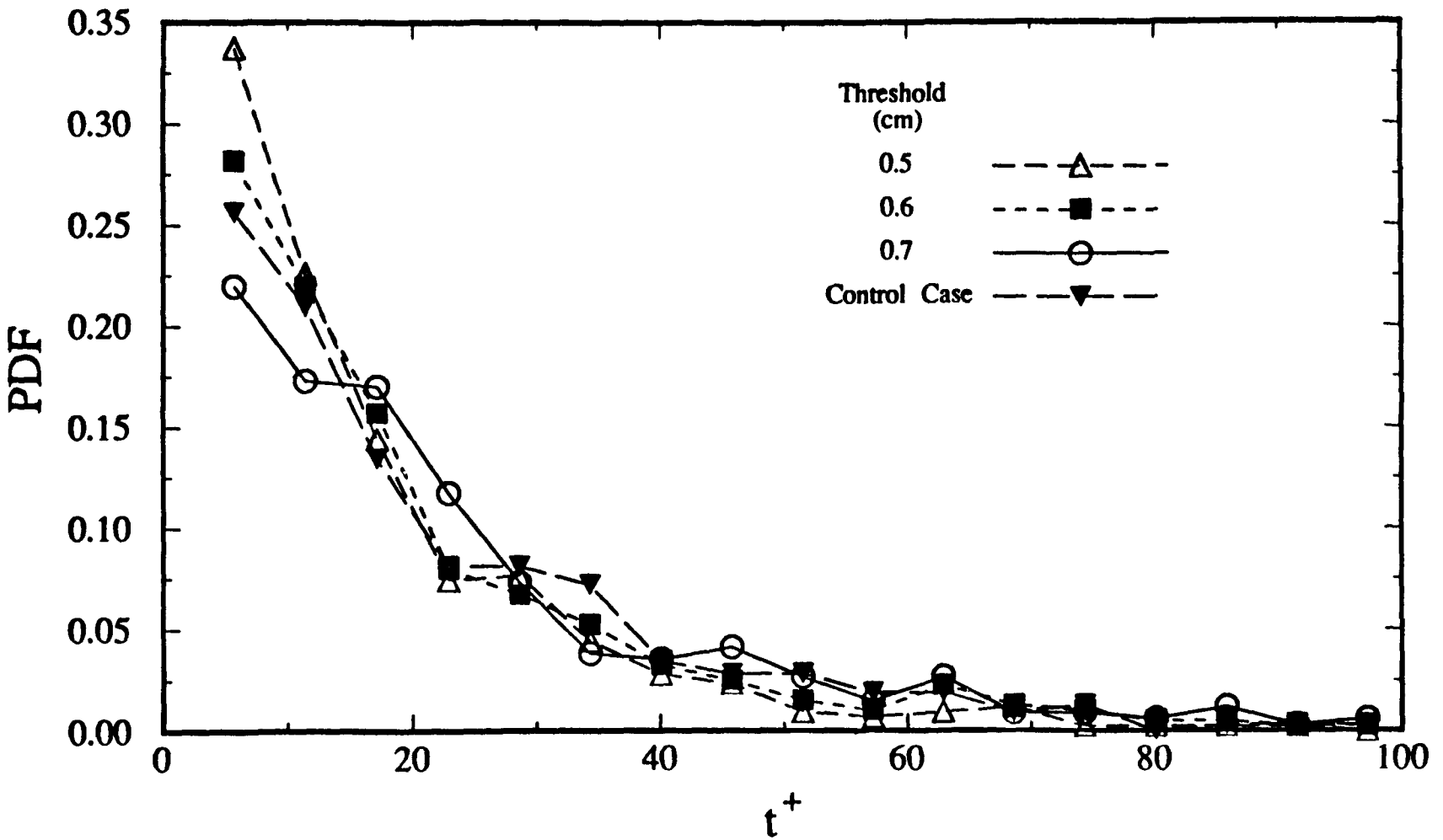


Figure 16 Comparison of PDF's of the Time-Duration of Structures from Film One (Plain Case) for Control Case and Three Tracking Thresholds

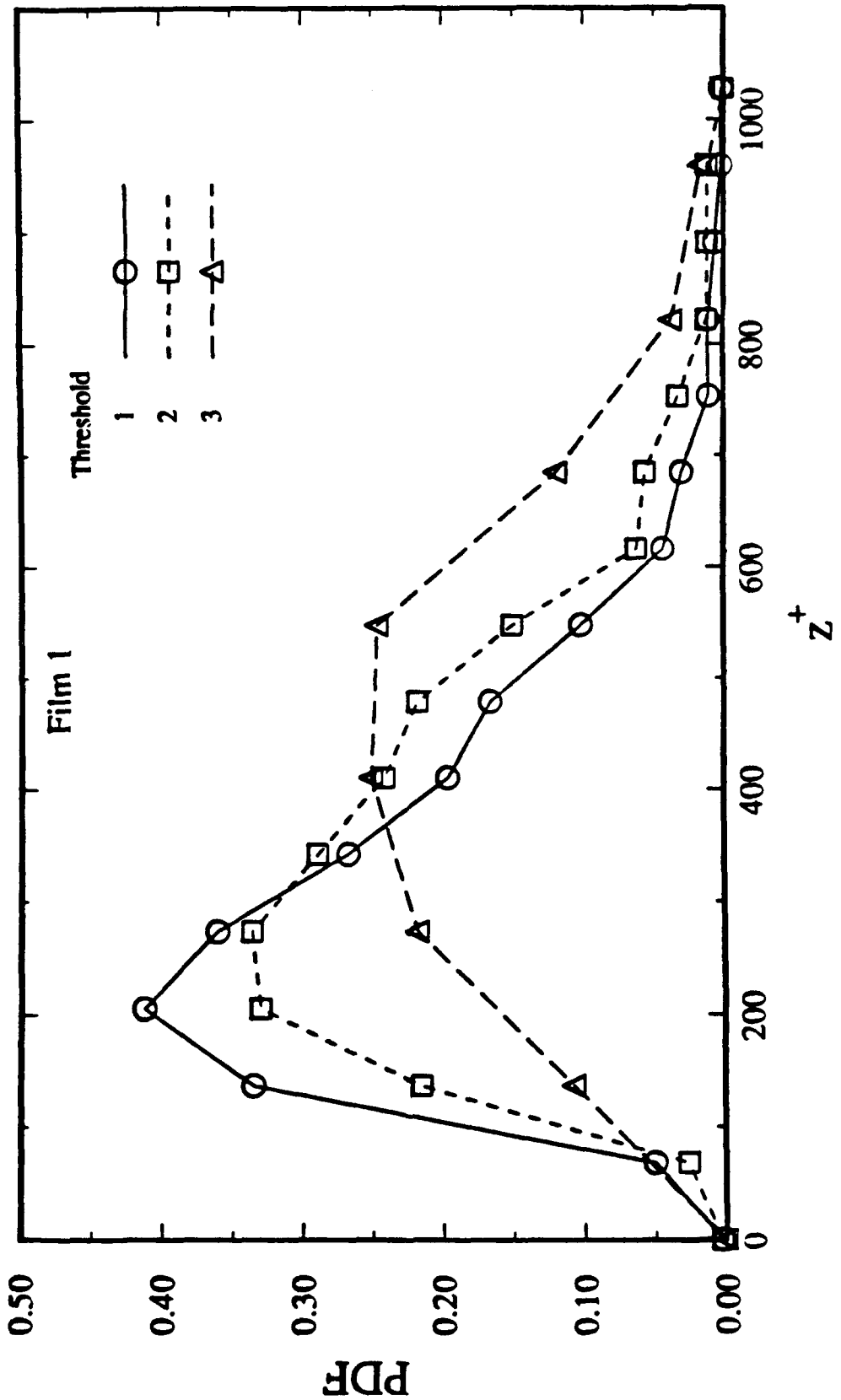


Figure 17 Threshold Effects on PDF's of Spanwise Spacing of Ejection Structures in Film One (Plain Case)

## VI. References


Adrian, R.J. 1991. *Particle-Imaging Techniques for Experimental Fluid Mechanics.* Annual Review of Fluid Mechanics, Vol. 23.

Antonia, R. A. and Bisset, D. K. 1990. *Spanwise Structure in the Near Wall Region of a Turbulent Boundary Layer.* J. Fluid Mech., Vol 210, pp. 437-458.

Blackwelder R.F. and Haritonidis, J.H. 1983. *Scaling of the bursting frequency in turbulent boundary layers.* J. Fluid Mech. Vol. 132, pp. 87-103

Blackwelder R.F. and Kovasznay L.S.G. 1972. *Time Scales and Correlations in a Turbulent Boundary Layer.* Physics of Fluids, Vol. 15, no. 9, pp. 1545-1554.

Corrsin S. and Kistler A.L. 1955. NACA Report no. 1244.

Guezennec, Y. G. 1985. *Documentation of Large Coherent Structures Associated With Wall Events in Turbulent Boundary Layers.* Ph.D. Thesis, Illinois Institute of Technology, Chicago, IL.

Guezennec, Y.G. and Nagib, H.N. 1990. *Mechanisms Leading to Net Drag Reduction in Manipulated Turbulent Boundary Layers.* AIAA Journal, Vol. 28, No. 2, pp. 245-252.

Hedley T.B. and Keffer J.F. 1974. *Turbulent/non-turbulent decisions in an intermittent flow.* J. Fluid Mech., Vol. 64, pp 625 - 644.

Kim, H.T., Kline, S.J. and Reynolds, W.C. 1971. *The production of turbulence near a smooth wall in a turbulent boundary layer.* J. Fluid Mech., Vol. 50, pp. 133-160.

Kovasznay, L.S.G., Kibens, V. and Blackwelder, R.F. 1970. *Large-scale motion in the intermittent region of a turbulent boundary layer.* J. Fluid Mech., Vol. 41, pp. 283.

Lekakis, I.C. 1988. *Coherent Structures in Fully Developed Turbulent Pipe Flow.* Ph.D. thesis, TAM Dept. University of Illinois at Urbana-Champaign.

Lu, S.S. and Willmarth, W.W. 1973. *Measurements of the Structure of the Reynolds Stress in a Turbulent Boundary Layer.* J. Fluid Mech., Vol. 60, pp. 481-511.

Luchik, T.S. and Tiederman, W.G. 1987. *Timescale and structure of ejections and bursts in turbulent channel flows.* J. Fluid Mech., Vol. 174, pp. 529-552.

McLean I.R. 1990. Ph.D. Thesis, University of Southern Cal., Los Angeles, CA

Naguib, A.M. and Wark, C.E. 1992. *Reynolds Number Effect on the Scales of Coherent Structures in a Turbulent Boundary Layer.* Submitted to Experiments in Fluids. Also M.S. thesis, A.M. Naguib, Illinois Institute of Technology.

Robinson, S.K. 1991. *The Kinematics of Turbulent Boundary Layer Structure.* NASA Technical Memorandum 103859, April 1991. Also Annual Review of Fluids, 1991. Also Ph.D. Thesis, Stanford University, 1990.

Spalart, P. R. 1988. *Direct Simulation of a Turbulent Boundary Layer Up to a* $Re_\theta = 1410$. J. Fluid Mech., Vol. 187, pp. 61-98.

Theodorsen, T. 1952. *Mechanism of Turbulence.* Proceedings Second Midwestern Conference on Fluid Mechanics, Bulletin No. 149. Ohio State University, Columbus, Ohio.

Wark, C. E. 1988. *Experimental Investigation of Coherent Structures in Turbulent Boundary Layers.* Ph. D. Thesis, Illinois Institute of Technology, Chicago, IL.

Wark, C.E., Hur, S.W. and Naguib, A.M. 1990. *Effects of Transition on the Reynolds-Stress Producing Events in a Turbulent Boundary layer.* Presented at the 28th Aerospace Sciences Meeting, January 8-11, 1990, Reno Nevada. Paper no. AIAA-90-0497.

Wark, C.E. & Nagib, H.M. 1991. *Experimental investigation of coherent structures in turbulent boundary layers.* J. Fluid Mech. Vol. 230, pp. 183-208.

Wark, C.E., Naguib, A.M. and Robinson, S.K. 1991. *Scaling of Spanwise Length Scales in a Turbulent Boundary Layer..* Presented at the 29th Aerospace Sciences Meeting, January 7-10, 1991, Reno Nevada. Paper no. AIAA-91-0235.

## VII. List of Publications, Theses and Presentations

*Experimental investigation of coherent structures in turbulent boundary layers.* C.E. Wark and H.M. Nagib. **J. Fluid Mech.**, Vol. 230, pp. 183-208.

*An Investigation of Wall-Layer Dynamics Using a Combined Temporal Filtering and Correlation Technique*, A.M. Naguib and C.E. Wark. **Accepted for publication in Journal of Fluid Mechanics.**

*Reynolds Number Effect on the Scales of Coherent Structures in a Turbulent Boundary Layer.* A.M. Naguib and C.E. Wark. Submitted to **Experiments in Fluids.**

*Structure of Turbulence Using PIV in a Wall-Bounded Shear Flow,* C.E. Wark, P.W. Offutt and R.J. Adrian. To be submitted to **Physics of Fluids.** Also presented as an invited lecture **at the 22nd Midwestern Mechanics Conference**, 6-9 October, 1991.

*Effects of Transition and Outer-Layer Intermittency on the Reynolds-Stress Producing Events in a Turbulent Boundary Layer,* S.W. Hur, **M.S. thesis,** Illinois Institute of Technology, December 1991. Advised by C.E. Wark

*Visualization of Dynamically Active Events in a Turbulent Boundary Layer,* D.W. Hathway, **M.S. thesis,** Illinois Institute of Technology, December, 1991. Advised by H.M. Nagib

*Relative Role and Interaction of Inner and Outer Layer Structures in the Near-Wall Region.* A.M. Naguib and C.E. Wark, **44th Annual Meeting, Division of Fluid Dynamics of the American Physical Society,** Arizona State University, 24-26 November 1991. Abstract CA 1.